Environmentally Assisted Cracking in Light Water Reactors

**Semiannual Report
January 1999 - June 1999**

Argonne National Laboratory

**U.S. Nuclear Regulatory Commission
Office of Nuclear Regulatory Research
Washington, DC 20555-0001**
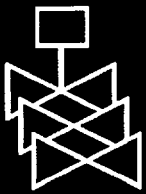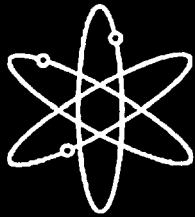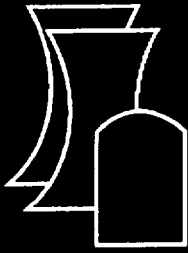
AVAILABILITY OF REFERENCE MATERIALS
IN NRC PUBLICATIONS

NRC Reference Material

As of November 1999, you may electronically access NUREG-series publications and other NRC records at NRC's Public Electronic Reading Room at www.nrc.gov/NRC/ADAMS/index.html.
Publicly released records include, to name a few, NUREG-series publications; *Federal Register* notices; applicant, licensee, and vendor documents and correspondence; NRC correspondence and internal memoranda; bulletins and information notices; inspection and investigative reports; licensee event reports; and Commission papers and their attachments.

NRC publications in the NUREG series, NRC regulations, and *Title 10, Energy,* in the Code of *Federal Regulations* may also be purchased from one of these two sources.
1. The Superintendent of Documents
   U.S. Government Printing Office
   P. O. Box 37082
   Washington, DC 20402–9328
   www.access.gpo.gov/su_docs
   202–512–1800
2. The National Technical Information Service
   Springfield, VA 22161–0002
   www.ntis.gov
   1–800–553–6847 or, locally, 703–605–6000

A single copy of each NRC draft report for comment is available free, to the extent of supply, upon written request as follows:
Address: Office of the Chief Information Officer,
           Reproduction and Distribution
             Services Section
           U.S. Nuclear Regulatory Commission
           Washington, DC 20555-0001
E-mail: DISTRIBUTION@nrc.gov
Facsimile: 301–415–2289

Some publications in the NUREG series that are posted at NRC's Web site address www.nrc.gov/NRC/NUREGS/indexnum.html are updated regularly and may differ from the last printed version.

Non-NRC Reference Material

Documents available from public and special technical libraries include all open literature items, such as books, journal articles, and transactions, *Federal Register* notices, Federal and State legislation, and congressional reports. Such documents as theses, dissertations, foreign reports and translations, and non-NRC conference proceedings may be purchased from their sponsoring organization.

Copies of industry codes and standards used in a substantive manner in the NRC regulatory process are maintained at—
           The NRC Technical Library
           Two White Flint North
           11545 Rockville Pike
           Rockville, MD 20852–2738

These standards are available in the library for reference use by the public. Codes and standards are usually copyrighted and may be purchased from the originating organization or, if they are American National Standards, from—
           American National Standards Institute
           11 West 42nd Street
           New York, NY 10036–8002
           www.ansi.org
           212–642–4900

The NUREG series comprises (1) technical and administrative reports and books prepared by the staff (NUREG–XXXX) or agency contractors (NUREG/CR–XXXX), (2) proceedings of conferences (NUREG/CP–XXXX), (3) reports resulting from international agreements (NUREG/IA–XXXX), (4) brochures (NUREG/BR–XXXX), and (5) compilations of legal decisions and orders of the Commission and Atomic and Safety Licensing Boards and of Directors' decisions under Section 2.206 of NRC's regulations (NUREG–0750).

Environmentally Assisted Cracking in Light Water Reactors

Semiannual Report
January 1999 - June 1999

Prepared by
O. K. Chopra, H. M. Chung, E. E. Gruber
T. F. Kassner, W. E. Ruther, W. J. Shack
J. L. Smith, W. K. Soppet, R. V. Strain

Argonne National Laboratory
9700 South Cass Avenue
Argonne, IL 60439

Previous Documents in Series

Environmentally Assisted Cracking in Light Water Reactors Semiannual Report

April—September 1985, NUREG/CR-4667 Vol. I, ANL-86-31 (June 1986).

October 1985—March 1986, NUREG/CR-4667 Vol. II, ANL-86-37 (September 1987).

April—September 1986, NUREG/CR-4667 Vol. III, ANL-87-37 (September 1987).

October 1986—March 1987, NUREG/CR-4667 Vol. IV, ANL-87-41 (December 1987).

April—September 1987, NUREG/CR-4667 Vol. V, ANL-88-32 (June 1988).

October 1987—March 1988, NUREG/CR-4667 Vol. 6, ANL-89/10 (August 1989).

April—September 1988, NUREG/CR-4667 Vol. 7, ANL-89/40 (March 1990).

October 1988—March 1989, NUREG/CR-4667 Vol. 8, ANL-90/4 (June 1990).

April—September 1989, NUREG/CR-4667 Vol. 9, ANL-90/48 (March 1991).

October 1989—March 1990, NUREG/CR-4667 Vol. 10, ANL-91/5 (March 1991).

April—September 1990, NUREG/CR-4667 Vol. 11, ANL-91/9 (May 1991).

October 1990—March 1991, NUREG/CR-4667 Vol. 12, ANL-91/24 (August 1991).

April—September 1991, NUREG/CR-4667 Vol. 13, ANL-92/6 (March 1992).

October 1991—March 1992, NUREG/CR-4667 Vol. 14, ANL-92/30 (August 1992).

April—September 1992, NUREG/CR-4667 Vol. 15, ANL-93/2 (June 1993).

October 1992—March 1993, NUREG/CR-4667 Vol. 16, ANL-93/27 (September 1993).

April—September 1993, NUREG/CR-4667 Vol. 17, ANL-94/26 (June 1994).

October 1993—March 1994, NUREG/CR-4667 Vol. 18, ANL-95/2 (March 1995).

April—September 1994, NUREG/CR-4667 Vol. 19, ANL-95/25 (September 1995).

October 1994—March 1995, NUREG/CR-4667 Vol. 20, ANL-95/41 (January 1996).

April—December 1995, NUREG/CR-4667 Vol. 21, ANL-96/1 (July 1996).

January 1996—June 1996, NUREG/CR-4667 Vol. 22, ANL-97/9 (June 1997).

July 1996—December 1996, NUREG/CR-4667 Vol. 23, ANL-97/10 (October 1997).

January 1997—June 1997, NUREG/CR-4667 Vol. 24, ANL-98/6 (April 1998).

July 1997—December 1997, NUREG/CR-4667 Vol. 25, ANL-98/18 (September 1998).

January 1998—June 1998, NUREG/CR-4667 Vol. 26, ANL-98/30 (December 1998).

July 1998—December 1998, NUREG/CR-4667 Vol. 27, ANL-99/11 (October 1999).

Environmentally Assisted Cracking in Light Water Reactors
Semiannual Report January 1999–June 1999

by

O. K. Chopra, H. M. Chung, E. E. Gruber, T. F. Kassner,
W. E. Ruther, W. J. Shack, J. L. Smith, W. K. Soppet, and R. V. Strain

Abstract

This report summarizes work performed by Argonne National Laboratory on fatigue and environmentally assisted cracking (EAC) in light water reactors (LWRs) from January 1999 to June 1999. Topics that have been investigated include (a) environmental effects on fatigue S–N behavior of primary pressure boundary materials, (b) irradiation–assisted stress corrosion cracking (IASCC) of austenitic stainless steels (SSs), and (c) EAC of Alloys 600 and 690. Fatigue tests have been conducted to study the effects of water chemistry on the fatigue life of austenitic SSs in LWR environments. Existing fatigue S–N data have been evaluated to establish the effects of temperature, dissolved oxygen, and strain rate on the fatigue life of these steels. Slow-strain-rate tensile tests and posttest fractographic analyses were conducted on several model SS alloys irradiated to $\approx 0.9 \times 10^{21}$ n·cm^{-2} (E > 1 MeV) in He at 289°C in the Halden reactor. The results have been used to determine the influence of alloying and impurity elements on the susceptibility of these steels to IASCC. Fracture toughness J–R curve tests were also conducted on two heats of Type 304 SS that were irradiated to ≈ 0.3 and 0.9×10^{21} n·cm^{-2} in the Halden reactor. Crack-growth-rate tests have been conducted on compact–tension specimens of Alloy 690 under cyclic loading to evaluate the enhancement of crack growth rates of these alloys in LWR environments.

Contents

Figures

Tables

Executive Summary

Environmental Effects on Fatigue Strain-versus-Life (S–N) Behavior of Primary Pressure Boundary Materials

The ASME Boiler and Pressure Vessel Code provides rules for the construction of nuclear power plant components. Appendix I to Section III of the Code specifies design fatigue curves for structural materials. However, the effects of light water reactor (LWR) coolant environments are not explicitly addressed by the Code design curves. Recent test data illustrate potentially significant effects of LWR environments on the fatigue resistance of carbon and low–alloy steels and austenitic stainless steels (SSs). Under certain loading and environmental conditions, fatigue lives of carbon and low–alloy steels can be a factor of $\approx$70 lower in an LWR environment than in air. These results raise the issue of whether the design fatigue curves in Section III are appropriate for the intended purpose.

A program is being conducted at Argonne National Laboratory (ANL) to develop data and models for predicting the effects of environment on fatigue design curves of pressure vessel and piping steels. Fatigue tests are being conducted to obtain data under conditions that are not included in the existing fatigue data base and to establish the effects of various loading and environmental variables on the fatigue S–N behavior of pressure–boundary steels. The existing fatigue S–N data have been analyzed to establish the effects of various material, loading, and environmental parameters on the fatigue life of carbon and low–alloy steels and austenitic SSs; the results have been summarized in NUREG/CR–6583 for carbon and low–alloy steels and in NUREG/CR–5704 for austenitic SSs.

The results to date for austenitic SSs indicate that environmental effects are more pronounced in low–dissolved oxygen (DO) (<0.01 ppm DO) than in high–DO (>0.1 ppm DO) water. In low–DO water, the fatigue life of austenitic SSs can be decreased up to a factor of 15 relative to that in air. The effects of environment increase with decreasing strain rate and saturate at $\approx$0.0004%/s. However, recent test results suggest that in high DO water the impurity level and the nature of the oxide film have a very strong effect on fatigue life of austenitic SSs.

During the present reporting period, the experimental effort has been focused on the effects of water chemistry on the fatigue lives of austenitic SSs. This report summarizes the data obtained on Type 304 SS in high–purity water at 288°C and $\approx$0.75% strain range to study the effect of electrochemical potential (ECP), conductivity, and DO content of water on the fatigue life of the steel. The results indicate that in high–DO water, environmental effects are moderate (less than a factor of 2 decrease in life) when conductivity is maintained at <0.1 μS/cm and the ECP of the steel has reached a stable value. For fatigue tests in high–DO water, the SS specimens must be soaked for $\approx$5 days for the ECP of the steel to reach a stable value. In low–DO water, the additions of Li and B, or low conductivity, or preexposing the specimen for $\approx$5 days before the test, or dissolved H have no effect on the fatigue life of austenitic SSs.

Irradiation-Assisted Stress Corrosion Cracking of Austenitic Stainless Steels

Slow-strain-rate tensile (SSRT) tests in simulated BWR water (DO $\approx$8 ppm) were conducted on model austenitic SS alloys that were irradiated at 289°C in He in the Halden

boiling-heavy-water reactor to a fluence of $\approx 0.9 \times 10^{21}$ n·cm^{-2} (E > 1 MeV). Fractographic analysis by scanning electron microscopy (SEM) was conducted to determine the susceptibility to irradiation-assisted stress corrosion cracking (IASCC) as manifested by the degree of transgranular and intergranular fracture surface morphology. Heat-to-heat variations in ductility and susceptibilities of the irradiated steels to intergranular and transgranular stress corrosion cracking (IGSCC and TGSCC) were very significant. This observation indicates that heat-to-heat variation in crack growth rate (CGR) could also be strong. A Type 304 SS alloy that contains a high concentration of O exhibited high susceptibility to IGSCC. A few Type 304 SS alloys that contain high concentrations of Si in the range of 1.1–1.5 wt.% exhibited negligible susceptibility to IGSCC. The beneficial effect of a high concentration of Cr was very significant, that is, alloys that contain <15.5 wt.% Cr exhibited relatively higher susceptibility to IASCC, whereas an alloy that contains >21 wt.% Cr exhibited relatively lower susceptibility than the other alloys.

Certain safety-related core internal structural components accumulate very high levels of irradiation damage (20-100 displacement per atom or dpa) by the end of life. Current data bases for and mechanistic understanding of the degradation of such highly irradiated components, however, are not adequate. A key question is the nature of irradiation-assisted intergranular cracking at very high dose, i.e., purely mechanical failure or SCC. To provide a better understanding of IASCC at very high fluence, hot-cell tests and microstructural characterization were performed on Type 304 SS specimens obtained from the hexagonal fuel can of the decommissioned EBR-II reactor after irradiation to ≈ 50 dpa at $\approx 370°C$. Slow-strain-rate tensile tests were conducted at 289°C in air and water at several levels of ECP, and microstructural characteristics were analyzed by scanning and transmission electron microscopies. Significant twinning occurred when the material was deformed. It exhibited surprisingly high ductility in air, but was susceptible to severe intergranular stress corrosion cracking (IGSCC) at high ECP. Low levels of DO and ECP were effective in suppressing the susceptibility of the heavily irradiated material to IGSCC. However, although IGSCC was suppressed, the material was susceptible to dislocation channeling at low ECP, and this susceptibility led to poor work-hardening capability and low ductility.

Fracture toughness J–R curve tests have been conducted on two commercial and two laboratory heats of Type 304 SS that were irradiated to fluence levels of ≈ 0.3 and 0.9×10^{21} n·cm^{-2} (E > 1 MeV) at $\approx 288°C$ in a He environment in the Halden boiling–heavy–water reactor. The tests were performed on 1/4–T compact tension (CT) specimens in air at 288°C and crack extensions were determined by both DC potential and elastic unloading compliance techniques. Neutron irradiation at 288°C to 0.9×10^{21} n·cm^{-2} decrease the fracture toughness of all of the steels. Minor differences in the composition of the steels, e.g., differences in Ni or Si content, have little or no effect on the fracture toughness of irradiated steels. The commercial heats exhibited fracture toughness that is superior to the fracture toughness of the laboratory heats. For steels irradiated to 0.9×10^{21} n·cm^{-2}, the J_{Ic} values are 326 and 331 kJ/m^2, respectively, for heats C16 and C19, and 36 and 38 kJ/m^2, respectively, for heats L2 and L20.

Environmentally Assisted Cracking of Alloys 600 and 690 in Simulated LWR Water

To evaluate the resistance of Alloys 600 and 690 to environmentally assisted cracking (EAC) in LWR coolant environment, fracture-mechanics CGR tests are being conducted in air and water environments on CT specimens of several heats of these alloys under annealed and

under annealed and thermally treated conditions. A statistical analysis of the results was used to develop correlations for predicting CGRs of the materials as a function of stress intensity, stress ratio, and DO levels. However, because the experimental data were obtained for only a single rise time, i.e., frequency, alternate forms for the correlations have also been developed to extrapolate the results to other rise times.

The CGRs in the low–C heat of Alloy 600 do not appear to be sensitive to either heat treatment or DO level, whereas the CGRs in the high–C heats show a strong environmental enhancement in high–DO environments. The results are inconclusive for the high–C Alloy 600 in low–DO environments. Alloy 690 shows only a modest environmental enhancement in low–DO environments; environmental effects appear to be independent of the loading conditions as long as $CGR_{air} \geq 10^{-11}$ s^{-1}. The CGRs in Alloy 690 in high–DO water show some environmental enhancement for loading conditions that correspond to low CGRs in air.

The crack growth data for Alloy 600 and 690 specimens under constant load in high–DO water (i.e., ≈300 ppb DO) show little or no effect of the stress intensity factor K on growth rates at K values of 27–30 MPa·m$^{1/2}$. For Alloy 600, the CGRs are influenced by thermal treatment; growth rates for the hot–worked Alloy 600 are a factor of ≈5 greater than those for the hot–worked + thermally treated Alloy 600. The addition of sulfate increased the CGRs of Alloy 600 by a factor of 3–7 under both heat treatment conditions. The CGRs for Alloy 690 range between ≈2 x 10^{-12} and 6 x 10^{-12} m/s; however, these values may be below the sensitivity of the crack–length monitoring system. Also, the addition of sulfates exerted no effect on the growth rates of Alloy 690.

The experimental effort during the current reporting period was focused on fatigue CGRs of Alloy 690 in high–purity water at 289°C. Crack growth tests have been conducted on Alloy 690 under cyclic loading in high–purity water with ≈350 ppm DO at 289°C, load ratio R = 0.7, ΔK = 11.5 MPa·m$^{1/2}$, and rise times of 12, 60, 300, and 1000 s. The results indicate that the CGRs of Alloy 690 in high–DO water are a factor of ≈4 greater than those in air.

Acknowledgments

1 Introduction

The U.S. Nuclear Regulatory Commission (NRC) and its predecessor, the U.S. Atomic Energy Commission, have conducted research programs that address the aging of reactor components. The results of the research have been used to evaluate and establish regulatory guidelines to ensure acceptable levels of reliability for light water reactor (LWR) components. The products of this program have been technical reports, methodologies for evaluating licensee submittals, and other inputs to the regulatory process. The results have led to the resolution of regulatory issues, as well as to the development, validation, and improvement of regulations and regulatory guides. The present research on the effects of simulated reactor coolant environments on cracking of reactor components was initiated to resolve the remaining critical technical issues related to cracking phenomena in LWR components. Initially, this project addressed cracking of boiling water reactor (BWR) pipes. Subsequently, in response to requests from the NRC Division of Nuclear Reactor Regulation (NRR) for assistance in dealing with developing cracking problems in aging reactors, the focus shifted to other problems in environmentally assisted cracking (EAC) of LWR components.

The overall objective of this program is to provide data and physical models to be used by the NRC staff in assessing environmentally assisted degradation of primary pressure boundary components in LWRs. The current research is focused on four tasks:

(a) *Environmental effects on fatigue, crack growth, and stress corrosion cracking*
Fatigue and EAC of piping, pressure vessels, and core components in LWRs are important concerns during plant operation and for extended reactor lifetimes. The degradation processes in U.S. reactors include fatigue, intergranular stress corrosion cracking (IGSCC), and propagation of fatigue or stress corrosion cracks that are initiated in the weld-sensitized heat-affected zones of stainless steel (SS) components. Occurrences of mechanical–vibration– and thermal–fluctuation– induced fatigue failures in LWR plants have also been documented. The objective of this task is to improve fatigue design curves and assess the additivity of fatigue damage in piping and vessel steels under load histories that are typical for LWR components. The results of this work will be used to assess industry fatigue evaluations that are related to license renewal.

(b) *Component vulnerability to irradiation-assisted stress corrosion cracking*
Irradiation–assisted stress corrosion cracking (IASCC) of in–core components in both BWRs and pressurized water reactors (PWRs) is becoming a more common problem as reactors age. The general pattern of the observed failures indicates that, as nuclear plants age and neutron fluence increases, many apparently nonsensitized austenitic materials become susceptible to intergranular failure by IASCC. Some of these failures have been reported for components that are subjected to relatively low or negligible stress levels, e.g., control–blade sheaths and handles and instrument dry tubes of BWRs. Although most failed components can be replaced, it would be very difficult or impractical to replace some safety–significant structural components, such as the BWR top guide, core plate, and shroud. The objective of this task is to provide data and models that are needed to assess industry analyses of the likelihood of degradation and failure of core internal components that are due to IASCC, and to evaluate licensee submissions that are related to inspection and remediation.

(c) *Cracking of nickel alloy components of LWR primary systems*
Internal components of reactor vessels are made of Ni-based alloys, e.g., Alloys 600, X750, and 182, which are susceptible to IGSCC. The causes and mechanisms of this cracking are not adequately understood, and the uncertainty is increased when licensee submissions are evaluated for factors such as damage accumulation and inspection intervals. The objective of this task is to provide technical data on the effects of cracks in Ni-alloy components on the residual life, inspection, and repair of the components. The results will be used to support NRR staff assessments of industry's crack-growth models, and potential detection and mitigation measures.

(d) *Assessment of industry's crack-growth models*
This task has two objectives. The first is to perform an independent evaluation of models that are used by industry to establish inspection intervals and repair criteria. The second objective is to perform more detailed analyses of flaw acceptance criteria.

Research during this six-month reporting period has focused on fatigue of austenitic SSs, fracture toughness J–R curve tests in air, and IASCC during slow-strain-rate tensile (SSRT) tests (in simulated BWR water) of SS specimens that were irradiated to fluence levels of ≈0.3 and 0.9×10^{21} n·cm^{-2} (E > 1 MeV) at 288°C in the Halden reactor, and EAC of Alloys 600 and 690 in high-purity oxygenated water.

2 Environmental Effects on Fatigue Strain-versus-Life (S–N) Behavior of Primary Pressure Boundary Materials

Experience with operating nuclear power plants worldwide reveals that many failures can be attributed to fatigue; examples include piping components, nozzles, valves, and pumps.[1-3] In most cases, these failures have been associated with thermal loading that is due to thermal stratification or thermal striping, or with mechanical loading that is due to vibratory loading. Significant thermal loadings due to flow stratification were not included in the original design basis analysis. The effects of these loadings may also have been aggravated by corrosion effects that are due to exposure to high-temperature aqueous environments. Fatigue cracks have been observed in pressurizer surge lines in PWRs (NRC Bulletin No. 88-11), and in feedwater lines connected to nozzles of pressure vessels in BWRs and steam generators in PWRs (NRC IE Bulletin, 79-13; NRC Information Notice 93-20). These cracks have been attributed to corrosion fatigue (NRC IE Bulletin, 79-13) or strain-induced corrosion cracking[4] caused by cyclic loading that is due to thermal stratification during start-up (hot standby) and shutdown periods.

2.1 Effects of Water Chemistry on the Fatigue Life of Austenitic Stainless Steels in LWR Coolant Environments (J. L. Smith, O. K. Chopra, and W. J. Shack)

2.1.1 Introduction

Cyclic loading on a structural component occurs because of changes in the mechanical and thermal loading as the system goes from one set of pressure, temperature, moment, and force load to any other load set. For each pair of load sets, an individual fatigue usage factor is determined by the ratio of the number of cycles anticipated during the lifetime of the component to the allowable cycles. Figures I-9.1 through I-9.6 of Appendix I to Section III of the ASME Boiler and Pressure Vessel Code[5] specify fatigue design curves that define the allowable number of cycles as a function of applied stress amplitude. The cumulative usage factor (CUF) is the sum of the individual usage factors. Section III of the ASME Code requires that the CUF at each location not exceed 1.

The Code design fatigue curves were based on strain-controlled tests of small polished specimens at room temperature in air. In most studies, the fatigue life of a test specimen is defined as the number of cycles for the tensile stress to drop 25% from its peak value, which corresponds to an ≈3-mm-deep crack. Consequently, fatigue life N represents the number of cycles required to initiate a crack that is ≈3 mm deep. The best-fit curves to the experimental data are expressed in terms of the Langer equation[6] of the form

$$\varepsilon_a = B(N)^{-b} + A, \tag{1}$$

where ε_a is strain amplitude and A, B, and b are parameters of the model. Equation 1 may be written in terms of stress amplitude S_a, where stress amplitude is the product of strain amplitude ε_a and elastic modulus, i.e., $S_a = E\varepsilon_a$. The design fatigue curves were obtained by first adjusting the best-fit curves for the effects of mean stress and then decreasing the adjusted curves by a factor of 2 on stress or 20 on cycles, whichever was more conservative, at each point on the adjusted curve. As described in the Section III criteria document,[7] these factors were intended to account for the differences and uncertainties in relating the fatigue

lives of laboratory test specimens to those of actual reactor components. The factor of 20 on cycles is the product of three subfactors: 2 for scatter of data (minimum to mean), 2.5 for size effects, and 4 for surface finish, atmosphere, etc. "Atmosphere" was intended to reflect the effects of an industrial environment rather than the controlled environment of a laboratory. The factors of 2 and 20 are not safety margins but rather conversion factors that must be applied to the experimental data to obtain reasonable estimates of the lives of actual reactor components; in a benign environment, some fraction of the factor may represent a safety margin.

Subsection NB-3121 of Section III of the Code states that the data on which the fatigue design curves (Figs. I-9.1 through I-9.6) are based did not include tests in the presence of corrosive environments that might accelerate fatigue failure. Article B-2131 in Appendix B to Section III states that the owner's design specifications should provide information about any reductions to fatigue design curves that are required because of environmental conditions. Recent fatigue strain-vs.-life (S–N) data illustrate the potentially significant effects of LWR coolant environments on the fatigue resistance of carbon steels (CSs), low–alloy steels (LASs),[8-20] and austenitic SSs,[21-31] (Fig. 1). Under certain loading and environmental conditions, fatigue lives of test specimens fall below the ASME Code fatigue design curves.
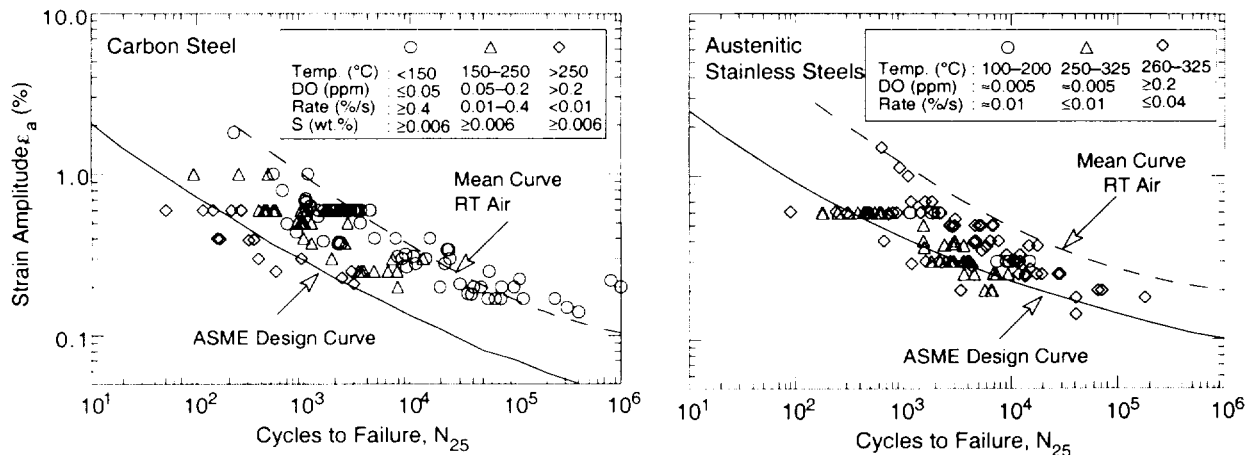
Figure 1. Fatigue S–N data for CS and austenitic SS in water; RT = room temperature

A program is being conducted at Argonne National Laboratory (ANL) to develop data and models for predicting the effects of environment on fatigue design curves of pressure vessel and piping steels. Fatigue tests are being conducted to obtain data under conditions that are not included in the existing fatigue data base and to establish the effects of various loading and environmental variables on the fatigue S–N behavior of pressure boundary steels. The existing fatigue S–N data have been analyzed to establish the effects of various material, loading, and environmental parameters on the fatigue life of carbon and low–alloy steels and austenitic SSs; the results have been summarized in NUREG/CR-6583[18] for carbon and low–alloy steels, and in NUREG/CR-5704[31] for austenitic SSs. Under certain environmental and loading conditions, fatigue lives of CSs can be a factor of 70 lower in the LWR environment than in air.[11,18-20] Therefore, the margins in the ASME Code may be less conservative than originally intended.

The results to date for austenitic SSs indicate that environmental effects are more pronounced in low–dissolved-oxygen (DO) (<0.01 ppm DO) than in high–DO (>0.1 ppm DO)

water. In low–DO water, the fatigue life of austenitic SSs can be decreased up to a factor of 15 relative to that in air. The effects of environment increase with decreasing strain rate and saturate at ≈0.0004%/s. However, recent test results suggest that in high–DO water, the impurity level and the nature of the oxide film have a very strong effect on fatigue life of austenitic SSs.

During the present reporting period, the experimental effort has been focused on the effects of water chemistry on the fatigue lives of austenitic SSs. This report summarizes the data obtained on Type 304 SS in high–purity water at 288°C and ≈0.75% strain range to study the effect of electrochemical potential (ECP), conductivity, and DO content in water on fatigue life of the steel.

2.1.2 Experimental

Fatigue tests have been conducted on Type 304 SS in air, and in simulated PWR and high–DO (≈0.8 ppm DO) water at 288°C. The composition of the steel is given in Table 1. Smooth cylindrical specimens with a 9.5-mm diameter and 19-mm gauge length were used for the fatigue tests (Fig. 2). A 1-μm surface finish was applied in the axial direction on the specimen gauge length to prevent circumferential scratches that might act as sites for crack initiation.

Table 1. Composition (wt.%) of Type 304 SS used for fatigue tests

Material	Heat	Source	C	P	S	Si	Cr	Ni	Mn	Mo	N
Type 304[a]	30956	Vendor	0.060	0.019	0.007	0.48	18.99	8.00	1.54	0.44	0.100

[a]Solution-annealed at 1050°C for 0.5 h.
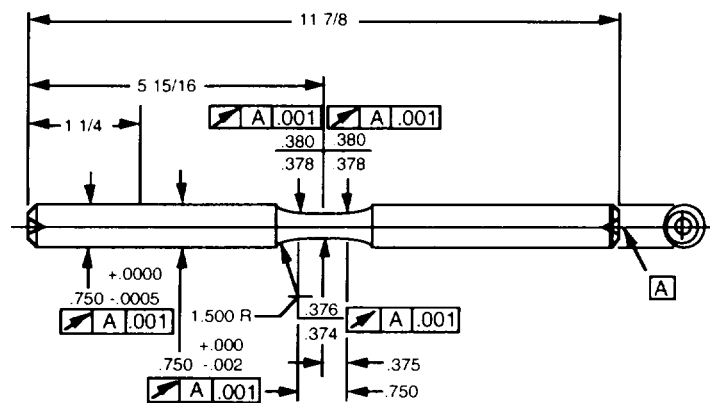
Figure 2. Configuration of fatigue test specimen (all dimensions in inches)

Tests in water were conducted in a 12-mL autoclave with a recirculating or once-through water system (Fig. 3) that consists of a 132-L closed feedwater storage tank, a Pulsafeeder™ high–pressure pump, regenerative heat exchanger, autoclave preheater, test autoclave, ECP cell, back-pressure regulator, ion exchange bed, 0.2 μm filter, and return line to the tank. Water is circulated at a rate of ≈10 mL/min and a system pressure of 9 MPa. The autoclave is constructed of Ti–lined Type 316 SS. The supply tank and most of the low–temperature piping are Type 304 SS; in some systems, the heat exchanger tubing and connections to the

autoclave and ECP cell are Ti. For corrosion fatigue tests in low–DO simulated PWR environments, the ECP cell and the ion–exchange filter in the return line from the autoclave to the water supply tank are both by–passed during recirculation. For a once–through water system, water from the back–pressure regulator is released to the drain.

The DO level in the water was established by bubbling N that contains 1–2% O through deionized water in the supply tank. The deionized water was prepared by passing purified water through a set of filters that comprise a C filter, an Organex–Q filter, two ion exchangers, and a 0.2–μm capsule filter. Water samples were collected periodically to measure pH, resistivity, and DO concentration. When the desired concentration of DO was attained, the N/O gas mixture in the supply tank was maintained at a 20–kPa overpressure. After an initial transition period during which an oxide film develops on the fatigue specimen, the DO level and the ECP in the effluent water remained constant during the test. For austenitic SS specimens, the transition period extended for 3–5 days. Although the difference between the DO levels in the feedwater and effluent water is >0.1 ppm, the difference between the DO levels at the inlet and outlet of the autoclave is ≈0.02 ppm. Test conditions are described in terms of the DO in effluent water.

1. Cover–gas supply tank
2. High-pressure regulator
3. Low-pressure regulator
4. Vent to air valve
5. Pressure relief valve
6. Water supply tank
7. Main water shutoff valve
8. Pulsafeeder high–pressure pump
9. Check valve
10. High-pressure gauge
11. Heat exchanger
12. Preheat exchanger
13. MTS load cell
14. MTS hydraulic collet grips
15. Displacement LVDT
16. Pipe autoclave
17. Control and measuring thermocouples
18. Fatigue test specimen
19. Resistance heaters
20. MTS servovalve
21. MTS hydraulic actuator
22. ECP cell
23. Platinum electrode
24. ECP thermocouple
25. ECP heater
26. Specimen electrode
27. Reference electrode
28. Mity Mite™ back–pressure regulator
29. Orbisphere dissolved–oxygen meter
30. MTS electrohydraulic controls
31. Resistance heater controls
32. Cover gas purifier
33. Recirculation pump
34. Demineralizer
35. 0.2 μm filter

Figure 3. Schematic diagram of recirculating autoclave system for fatigue tests in water

Simulated PWR water was obtained by dissolving boric acid and lithium hydroxide in 20 L of deionized water before adding the solution to the supply tank. The DO in the deionized water was reduced to <10 ppb by bubbling N through the water. A vacuum was drawn on the tank cover gas to speed deoxygenation. After the DO was reduced to the desired level, a 34-kPa overpressure of H was maintained to provide ≈2 ppm dissolved H (or ≈23 cm^3/kg) in the feedwater.

An Orbisphere meter and CHEMetrics™ ampules were used to measure the DO concentrations in the supply and effluent water. The redox and open-circuit corrosion potentials were monitored at the autoclave outlet by measuring the ECPs of platinum and an electrode of the test material, respectively, against a 0.1-M KCl/AgCl/Ag external (cold) reference electrode. The measured ECPs, $E_{(meas)}$ (mV), were converted to the standard H electrode (SHE) scale, $E_{(SHE)}$ (mV), by solving the polynomial expression[35]

$$E_{(SHE)} = E_{(meas)} + 286.637 - 1.0032(\Delta T)$$
$$+ 1.7447 \times 10^{-4}(\Delta T)^2 - 3.03004 \times 10^{-6}(\Delta T)^3, \tag{2}$$

where ΔT (°C) is the test temperature of the salt bridge in the reference electrode minus the ambient temperature.

All tests were conducted at 288°C, with fully reversed axial loading (i.e., R = –1) and a triangular or sawtooth waveform. The tests in water were performed under stroke control, wherein the specimen strain was controlled between two locations outside the autoclave. Tests in air were performed under strain control with an axial extensometer; the stroke at the location used to control the water tests was also recorded. Information from the air tests was
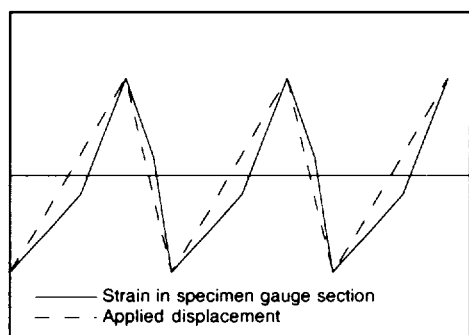
Figure 4.
Total applied displacement and strain in specimen gauge section during stroke-controlled tests with sawtooth waveform

used to determine the stroke required to maintain constant strain in the specimen gauge. To account for cyclic hardening of the material, the stroke that was needed to maintain constant strain was gradually increased during the test. Figure 4 shows the actual strain in the specimen gauge section during a stroke-controlled test with a sawtooth waveform. The fraction of applied displacement that is applied to the specimen gauge section is not constant but varies with loading strain. Consequently, the loading rate also varies during the fatigue cycle; it is lower than the applied strain rate at strain levels below the elastic limit and higher at larger strains.

2.1.3 Results

The fatigue results obtained to date on Type 304 SS in air and LWR environments are summarized in Table 2. The fatigue life N_{25} is defined as the number of cycles for tensile

stress to drop 25% from its peak value. Fatigue lives defined by other criteria, e.g., a 50% decrease in peak tensile stress or complete failure, may be converted to an N_{25} value using the equation

$$N_{25} = N_X / (0.947 + 0.00212\ X),$$
(3)

where X is the failure criterion, i.e., 25, 50, or 100% decrease in peak tensile stress. For tests in water, the DO level and ECPs of Pt and SS electrodes represent the values in the effluent; the pH and conductivity of water were both measured in the supply tank.

The results from the present study and data obtained elsewhere indicate that the fatigue lives of austenitic SSs are decreased in LWR environments; the reduction depends on strain rate, level of DO in water, and temperature.[22-31] The effects of LWR environments on the fatigue life of wrought materials are comparable for Types 304, 316, and 316NG SSs. The significant results and threshold values of critical parameters are summarized below.

Table 2. Fatigue test results for Type 304 austenitic SS at 288°C

Test No.	Env.	DO[a] (ppb)	pH at RT	Conductivity[b] (μS/cm)	ECP[a] Pt mV (SHE)	ECP[a] Steel mV (SHE)	Ten. Rate (%/s)	Comp. Rate (%/s)	Stress Range (MPa)	Strain Range (%)	Life N_{25} (Cycles)
1801	Air	–	–	–	–	–	4.0E-1	4.0E-1	419.2	0.76	24,500
1805	Air	–	–	–	–	–	4.0E-3	4.0E-1	467.9	0.76	14,410
1804	Air	–	–	–	–	–	4.0E-1	4.0E-1	382.8	0.51	61,680
1817	Air	–	–	–	–	–	4.0E-3	4.0E-1	421.7	0.51	42,180
1825	Air	–	–	–	–	–	4.0E-2	4.0E-1	394.4	0.30	>625,860
1846	Air	–	–	–	–	–	4.0E-2	4.0E-1	396.4	0.32	>316,000
1806	PWR[c]	4	6.0	18.87	-678	-675	4.0E-1	4.0E-1	428.9	0.73	11,500
1810	PWR[c]	5	6.4	18.89	-684	-681	4.0E-2	4.0E-1	447.6	0.77	5,800
1808	PWR[c]	4	6.4	18.87	-689	-686	4.0E-3	4.0E-1	468.3	0.77	2,850
1821	PWR[c]	2	6.5	22.22	-696	-693	4.0E-3	4.0E-1	474.3	0.76	2,420
1859	PWR[c]	2	6.5	18.69	-695	-692	4.0E-3	4.0E-1	471.7	0.77	2,420
1861	HP[d]	1	6.2	0.059	-597	-610	4.0E-3	4.0E-1	463.0	0.79	2,620
1862	HP[d]	2	6.2	0.058	-604	-603	4.0E-3	4.0E-1	466.1	0.78	2,450
1863	HP[e]	1	6.3	0.061	-442	-536	4.0E-3	4.0E-1	476.5	0.77	2,250
1829	PWR[c]	2	6.5	18.18	-701	-701	4.0E-4	4.0E-1	493.6	0.73	1,560
1834	PWR[c]	2	6.5	18.18	-707	-708	9.0E-5	4.0E-1	535.9	0.69	1,415
1807	PWR[c]	4	6.5	18.87	-681	-678	4.0E-1	4.0E-1	374.6	0.51	25,900
1823	PWR[c]	3	6.6	23.06	-697	-695	4.0E-3	4.0E-1	408.2	0.51	6,900
1826	PWR[c]	2	6.5	18.76	-707	-706	1.0E-2	4.0E-1	375.8	0.29	>89,860
1847	PWR[c]	5	6.5	18.87	-696	-692	1.0E-2	4.0E-1	388.9	0.32	>165,300
1852	HP[f]	790	6.1	0.061	239	153	4.0E-1	4.0E-1	429.1	0.74	10,800
1827	HP[e]	850	6.0	0.086	258	80	4.0E-3	4.0E-1	475.8	0.75	3,650
1853	HP[f]	880	6.1	0.059	252	159	4.0E-3	4.0E-1	466.5	0.76	12,300
1855	HP[f]	890	6.0	0.115	279	154	4.0E-3	4.0E-1	464.4	0.77	8,080
1856	HP[f]	870	6.2	0.074	276	167	4.0E-3	4.0E-1	473.6	0.75	10,450
1857	HP[f]	790	6.1	0.420	258	147	4.0E-3	4.0E-1	461.9	0.78	5,300
1860	HP[e]	810	6.1	0.560	277	129	4.0E-3	4.0E-1	468.3	0.77	3,050
1845	HP[f]	870	6.0	0.063	274	185	4.0E-4	4.0E-1	488.7	0.71	>7,310

[a]Measured in affluent.
[b]Measured in feedwater supply tank.
[c]Simulated PWR water containing 2 ppm Li, 1000 ppm B, and ≈2 ppm dissolved H
[d]High–purity water with H cover gas (≈2 ppm dissolved H), all other tests with N or N/1–2% O cover gas.
[e]High–purity water.
[f]Specimen soaked for ≈5 days prior to testing, all other tests soaked for 1 day.

- *Strain*: A minimum threshold strain is required for environmentally assisted decrease in fatigue life of austenitic SSs. Limited data suggest that the threshold strain range is between 0.32 and 0.36%.[24,30,31] Figure 5a shows the results of exploratory fatigue tests on Type 316 SS in low–DO water at 325°C, 1% strain range, and with waveforms in which the slow strain rate is applied during only a fraction of the tensile loading cycle.[24] The results indicate that a minimum threshold strain of ≈0.36% is required to produce an environmentally assisted decrease in fatigue life of the steel. During each cycle, relative damage due to slow strain rate is the same once the strain amplitude exceeds the threshold value.

- *Dissolved Oxygen in Water*: For wrought austenitic SSs, environmental effects on fatigue life are more pronounced in low–DO, i.e., <0.01 ppm DO, than in high–DO, i.e., ≥0.1 ppm DO, water.[23–30] The results also indicate that for fatigue tests in high–DO water, the conductivity of water and establishing stable environmental conditions have a strong effect on fatigue life of austenitic SSs. The fatigue lives of Type 304 SS in air, simulated PWR, and high–DO water at 288°C and ≈0.76% strain range are plotted as a function of strain rate in Fig. 5b. The recent data (triangles in Fig. 5b) indicate only a modest effect of environment on fatigue life in high–DO water, e.g., life is lower by a factor of ≈2 relative to that in air. The fatigue lives of earlier tests (diamonds in Fig. 5b) showed significant reduction in high–DO water. Test procedures for recent and earlier
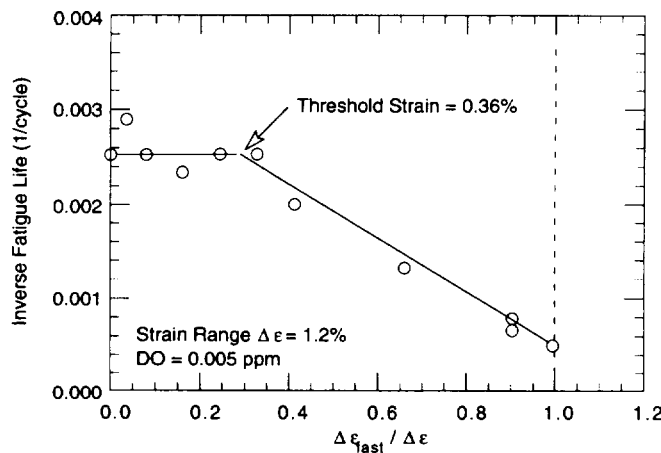
Figure 5a.
Results of strain rate change tests on Type 316 SS in low–DO water at 325°C
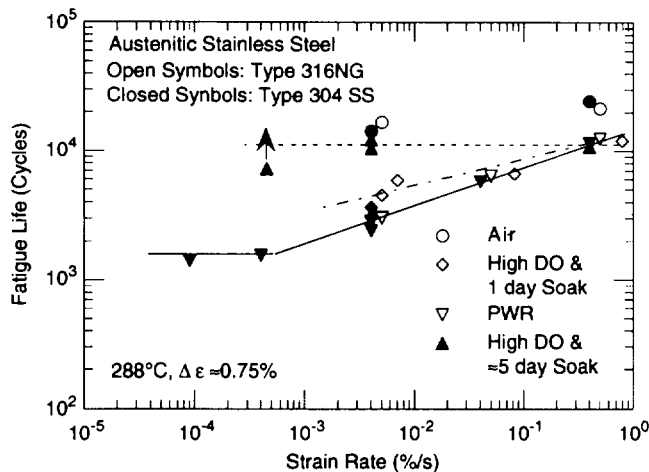
Figure 5b.
Dependence of fatigue life of austenitic SS on strain rate in low– and high–DO water

tests differed in two ways. In recent tests, the conductivity of water was controlled at ≈0.08 μS/cm compared to values between 0.15 and 0.5 μS/cm in earlier tests, and, in recent tests, the specimens were soaked for ≈5 days to allow the ECP of the steel electrode to reach a stable value, whereas in earlier tests, specimens were soaked for ≈24 h. Therefore, in earlier tests, the specimen ECP was typically ≈10 mV (or even negative) at the start of the test and gradually increased to 160 mV (SHE) during the initial period of 3–5 days, which corresponds to up to 2000 cycles.

The results of several tests on Type 304 SS in high–DO water at 288°C, ≈0.76% strain range, and 0.004%/s tensile strain rate, are plotted as a function of water conductivity in Fig. 6. The results indicate that environmental effects are moderate (less than a factor of 2 decrease in life) when conductivity is maintained at <0.1 μS/cm and the specimens have been soaked for ≈5 days to allow the ECP of the steel to reach a stable value. Figure 6 shows that although fatigue life is decreased by a factor of ≈2 when conductivity of water is increased from ≈0.07 to 0.4 μS/cm, the period for presoaking appears to have a larger effect on life than the conductivity of water.
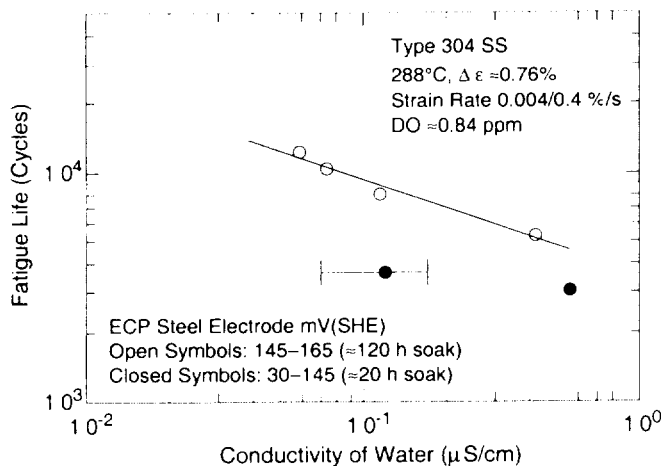
Figure 6.
Effects of conductivity of water and soak period on fatigue life of Type 304 SS in high–DO water

In low–DO water, addition of Li and B, or low conductivity, or soaking the specimen for ≈5 days before the test, or dissolved H, have no effect on fatigue life of austenitic SSs. The fatigue lives of Type 304 SS in water that contains <0.01 ppm DO at 288°C, ≈0.76% strain range, a slow/fast sawtooth waveform with 0.004%/s tensile strain rate, with or with-out the addition of Li and B, one- or five-day soak period, and with no dissolved H, range between 2250 and 2650 cycles; these tests are listed in Table 2 as tests number 1808–1863.

• *Strain Rate*: In high–DO water (conductivity <0.1 μS/cm and stable ECP of the steel), fatigue life is insensitive to changes in strain rate (dashed line in Fig. 5b). In low–DO water, fatigue life decreases logarithmically with decreasing strain rate below ≈0.4%/s (solid line in Fig. 5b); the effect of environment on life saturates at ≈0.0004%/s for wrought SSs.[23,24,28-30]

• *Temperature*: Existing data are too sparse to establish the effects of temperature on fatigue life over the entire range from room temperature to reactor operating temperatures. Limited data indicate that environmental effects on fatigue life are

minimal below 200°C and significant at temperatures above 250°C (Fig. 7);[23,24] life appears to be relatively insensitive to changes in temperature in the range of 250–330°C. The pressure vessel research council (PVRC) steering committee for CLEE (cyclic life and environmental effects) has proposed a ramp function to describe temperature effects on the fatigue lives of austenitic SSs;* environmental effects are moderate at temperatures below 180°C, significant above 220°C, and increase linearly from 180 to 220°C.
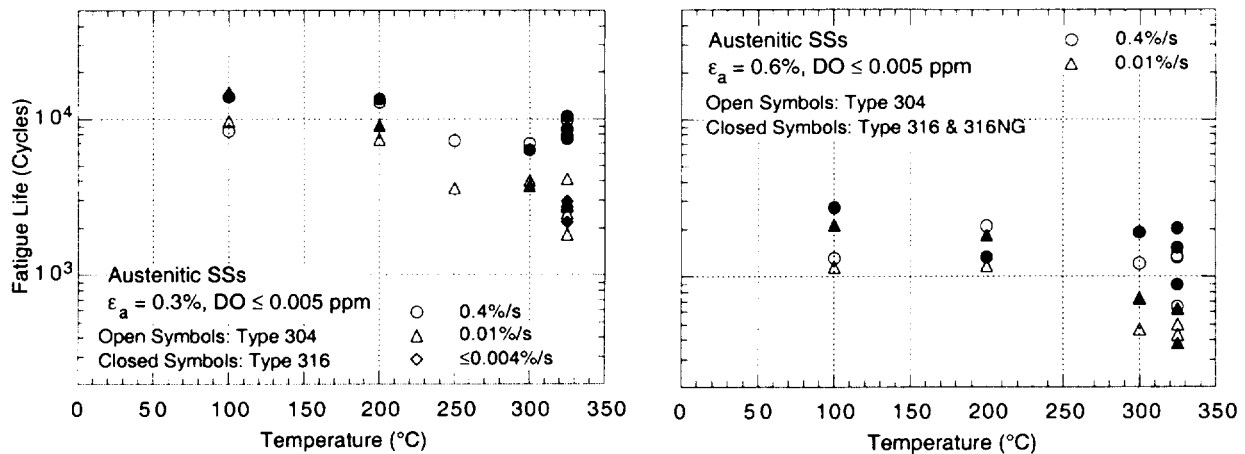
Figure 7. Change with temperature in fatigue lives of austenitic SSs in low–DO water

2.1.4 Conclusions

Fatigue tests have been conducted on Type 304 SS in high–purity water at 288°C to study the effects of water chemistry on the fatigue life of these steels. The results indicate that for wrought austenitic SSs, environmental effects on fatigue life are more pronounced in low–DO, i.e., < 0.01 ppm DO, than in high–DO, i.e., ≥ 0.1 ppm DO, water. In high–DO water, environmental effects are moderate (less than a factor of 2 decrease in life) when conductivity is maintained at < 0.1 μS/cm and ECP of the steel has reached a stable value. For fatigue tests in high–DO water, the SS specimens must be soaked for ≈5 days for the ECP of the steel to reach a stable value. In low–DO water, low conductivity, preexposing the specimen for ≈5 days before the test, dissolved H, and the addition of Li and B, have no effect on fatigue life of austenitic SSs. Additional fatigue tests are being conducted in high–DO water at 288°C to confirm these results.

---

*S. Yukawa, meeting of PVRC steering committee for CLEE, June 15, 1999, Columbus, OH.

3 Irradiation–Assisted Stress Corrosion Cracking of Austenitic Stainless Steels

3.1 Introduction

Failures of reactor core internal components have been observed after accumulation of fluence $> 0.5 \times 10^{21}$ n·cm^{-2} (E $>$ 1 MeV), or ≈ 0.7 dpa, in BWRs and at approximately one order of magnitude or higher fluences in some PWR components. The general pattern of the observed failures indicates that as nuclear plants age and neutron fluence increases, various nonsensitized austenitic SSs become susceptible to intergranular (IG) failure. Some components are known to have cracked under minimal applied stress. Although most failed components can be replaced (e.g., PWR baffle–former bolts), some safety–significant structural components (e.g., the BWR top guide, shroud, and core plate) would be very difficult or costly to replace. Therefore, the structural integrity of these components at high fluence has been a subject of concern, and extensive research has been conducted to provide an understanding of this type of degradation, which is commonly known as IASCC.[32-65]

Irradiation profoundly affects local coolant water chemistry and component microstructure. Neutron irradiation causes alteration of local microchemistry, microstructure, and mechanical properties of the core internal components, which are usually fabricated from ASTM Types 304, 304L, 316, or 348 SS. Irradiation produces defects, defect clusters, and defect-impurity complexes in grain matrices and alters the dislocation and dislocation loop structures, leading to radiation-induced hardening, and in many cases, flow localization via dislocation channeling. Irradiation also leads to changes in the stability of second–phase precipitates and the local alloy chemistry near grain boundaries, precipitates, and defect clusters. Grain–boundary microchemistry that is significantly different from bulk composition can be produced in association with not only radiation–induced segregation but also in association with thermally driven equilibrium and nonequilibrium segregation of alloying and impurity elements.

For many years, irradiation–induced grain–boundary depletion of Cr has been considered the primary metallurgical process that causes IASCC. Many investigators regard the similar dependence on water chemistry (i.e., oxidizing potential) of IGSCC of nonirradiated thermally sensitized material and of IASCC of BWR–irradiated solution–annealed material as the most important factor that supports the Cr–depletion mechanism. Other investigators have implicated radiation–induced segregation of ASTM–specified impurities, such as Si, P, S, and other minor impurities not specified in the ASTM specification. However, the understanding of the mechanism of IASCC still remains incomplete. In general, IASCC is characterized by strong heat-to-heat variation in susceptibility, in addition to strong effects of irradiation conditions, and material type and grade, even among materials of virtually identical chemical composition. These factors indicate that the grain-boundary Cr depletion cannot completely explain the mechanism of IASCC. Therefore, an irradiation testing program has been conducted to systematically investigate the effects of alloying and impurity elements (Cr, Ni, Si, P, S, Mn, C, and N) on the susceptibility of austenitic SSs to IASCC at several fluence levels. In a previous study,[66] SSRT testing and fractographic analysis were conducted on "low-fluence" specimens irradiated in the Halden reactor to $\approx 0.3 \times 10^{21}$ n·cm^{-2} (E $>$ 1 MeV). This report describes a continuation of the previous study and presents results that were obtained for "medium-fluence" specimens irradiated to $\approx 0.9 \times 10^{21}$ n·cm^{-2} (E $>$ 1 MeV) or ≈ 1.3 dpa. To

provide a better understanding of IASCC at very high fluence, hot-cell tests and microstructural characterization were also performed on Type 304 SS specimens obtained from the hexagonal fuel can of the decommissioned EBR-II reactor after irradiation to ≈50 dpa at ≈370°C. Results of SSRT tests and posttest microstructural analyses of the highly irradiated steel by scanning and transmission electron microscopy (SEM and TEM) are also presented.

3.2 Slow-Strain-Rate-Tensile Test of Model Austenitic Stainless Steels Irradiated in the Halden Reactor (H. M. Chung, W. E. Ruther, and R. V. Strain)

3.2.1 Specimen Irradiation and Test Procedure

In this task, 27 model austenitic SS alloys of Types 304, 304L, 316, 316L, and 348 SS were selected and irradiated in the Halden reactor in He at 289°C. Compositions of the 27 alloys, 19 fabricated in the laboratory and eight purchased commercially, are summarized in Table 3. Slow-strain-rate-tensile and 1/4–T compact-tension (CT) specimens were prepared

Table 3. Elemental composition of 27 commercial and laboratory model austenitic SS alloys irradiated in the Halden reactor

ANL ID[a]	Source Heat ID	Elemental Composition (wt.%)										
		Ni	Si	P	S	Mn	C	N	Cr	O	B	Mo or Nb
C1	DAN-70378	8.12	0.50	0.038	0.002	1.00	0.060	0.060	18.11	-	<0.001	-
L2	BPC-4-111	10.50	0.82	0.080	0.034	1.58	0.074	0.102	17.02	0.0065	<0.001	-
C3	PNL-C-1	8.91	0.46	0.019	0.004	1.81	0.016	0.083	18.55	-	<0.001	-
L4	BPC-4-88	10.20	0.94	0.031	0.010	1.75	0.110	0.002	15.80	-	<0.001	-
L5	BPC-4-104	9.66	0.90	0.113	0.028	0.47	0.006	0.033	21.00	-	<0.001	-
L6	BPC-4-127	10.00	1.90	0.020	0.005	1.13	0.096	0.087	17.10	0.0058	<0.001	-
L7	BPC-4-112	10.60	0.18	0.040	0.038	1.02	0.007	0.111	15.40	0.0274	<0.001	-
L8	BPC-4-91	10.20	0.15	0.093	0.010	1.85	0.041	0.001	18.30	-	<0.001	-
C9	PNL-C-6	8.75	0.39	0.013	0.013	1.72	0.062	0.065	18.48	-	<0.001	-
C10	DAN-23381	8.13	0.55	0.033	0.002	1.00	0.060	0.086	18.19	-	<0.001	-
L11	BPC-4-93	8.15	0.47	0.097	0.009	1.02	0.014	0.004	17.40	-	<0.001	-
C12	DAN-23805	8.23	0.47	0.018	0.002	1.00	0.060	0.070	18.43	-	<0.001	-
L13	BPC-4-96	8.18	1.18	0.027	0.022	0.36	0.026	0.001	17.40	-	<0.001	-
L14	BPC-4-129	7.93	1.49	0.080	0.002	1.76	0.107	0.028	15.00	0.0045	<0.001	-
L15	BPC-4-126	8.00	1.82	0.010	0.013	1.07	0.020	0.085	17.80	0.0110	<0.001	-
C16	PNL-SS-14	12.90	0.38	0.014	0.002	1.66	0.020	0.011	16.92	-	<0.001	-
L17	BPC-4-128	8.00	0.66	0.090	0.009	0.48	0.061	0.078	15.30	0.0092	<0.001	-
L18	BPC-4-98	8.13	0.14	0.016	0.033	1.13	0.080	0.001	18.00	-	<0.001	-
C19	DAN-74827	8.08	0.45	0.031	0.003	0.99	0.060	0.070	18.21	-	<0.001	-
L20	BPC-4-101	8.91	0.017	0.010	0.004	0.41	0.002	0.002	18.10	-	<0.001	-
C21[b]	DAN-12455	10.24	0.51	0.034	0.001	1.19	0.060	0.020	16.28	-	<0.001	Mo 2.08
L22[c]	BPC-4-100	13.30	0.024	0.015	0.004	0.40	0.003	0.001	16.10	-	<0.001	Mo 2.04
L23[d]	BPC-4-114	12.04	0.68	0.030	0.047	0.96	0.043	0.092	17.30	0.0093	<0.001	Nb 1.06
L24[e]	BPC-4-105	12.30	0.03	0.007	0.005	0.48	0.031	0.002	16.90	0.0129	<0.001	Nb 1.72
L25C3	BPC-4-133	8.93	0.92	0.020	0.008	1.54	0.019	0.095	17.20	0.0085	0.010	-
L26C19	BPC-4-131	8.09	0.79	0.004	0.002	0.91	0.070	0.089	17.20	0.0080	<0.001	-
L27C21	BPC-4-132	10.30	0.96	0.040	0.002	0.97	0.057	0.019	15.30	0.0058	0.030	Mo 2.01

[a]First letters "C" and "L" denote commercial and laboratory heats, respectively.
[b]Commercial-purity Type 316 SS.
[c]High-purity Type 316 SS.
[d]Commercial-purity Type 348 SS.
[e]High-purity Type 348 SS.

from the alloy products and were irradiated in the Halden reactor. Susceptibility to IASCC was determined by SSRT testing the irradiated specimens in BWR-simulated water and by posttest fractographic examination by SEM. After completion of the SSRT tests and fractographic analysis of specimens irradiated to a fluence of $\approx 0.3 \times 10^{21}$ n·cm^{-2} (E > 1 MeV), similar tests were conducted on alloys irradiated to the medium-fluence level of $\approx 0.9 \times 10^{21}$ n·cm^{-2} (E > 1 MeV).

All SSRT tests were conducted at 289°C in BWR-like deionized high-purity water that contained ≈ 8 ppm DO. The strain rate during all SSRT tests was kept constant at 1.65×10^{-7} s^{-1}. Concentration of DO, controlled by purging the deaerated water with an N/O mixture, was measured on the effluent side. Conductivity and pH of the water at room temperature were in the range of ≈ 0.06–0.07 µS/cm and 6.7-7.1, respectively. Electrochemical potential was measured at the effluent side at regular intervals.

3.2.2 Results of SSRT Test and Fractographic Analysis of Medium-Fluence Specimens

Slow-strain-rate tensile tests were conducted in water on 16 medium-fluence specimens irradiated to $\approx 0.9 \times 10^{21}$ n·cm^{-2} (E > 1 MeV). A summary of the results from the SSRT tests is presented in Table 4. The stress corrosion behavior is correlated with compositional characteristics of the alloys in Table 5. For the tested medium-fluence specimens, effects of the higher fluence on yield stress, maximum stress, uniform strain, total strains, percent IGSCC, and percent transgranular SCC (TGSCC) were significant. Figure 8 summarizes percent IGSCC of the medium-fluence alloys (fluence $\approx 0.9 \times 10^{21}$ n·cm^{-2}, E > 1 MeV) tested to date. Similar results for low-fluence specimens (fluence $\approx 0.3 \times 10^{21}$ n·cm^{-2}, E > 1 MeV) are also shown in the figure for comparison.

Table 4. Results of SSRT tests[a] and SEM fractography of model austenitic stainless steels irradiated in He at 289°C to fluence of $\approx 0.9 \times 10^{21}$ n·cm^{-2} (E > 1 MeV)

ID No.	SSRT No.	Feedwater Chemistry				SSRT Parameters				Fracture Behavior		
		Oxygen Conc. (ppm)	Average ECP (mV SHE)	Cond. at 25°C (µS·cm^{-1})	pH at 25°C	Yield Stress (MPa)	Max. Stress (MPa)	Uniform Elong. (%)	Total Elong. (%)	TGSCC (%)	IGSCC (%)	TGSCC + IGSCC (%)
L22-02	HR-17	8.0	+181	0.08	6.77	475	549	4.20	5.82	30	35	65
L11-02	HR-18	8.0	+191	0.08	6.55	820	856	0.43	1.65	50	14	64
L18-02	HR-19	8.0	+193	0.10	6.07	710	755	3.98	5.05	38	14	52
L20-02	HR-28		Test in 289°C Air			826	845	0.31	2.09	0	0	0
L20-05	HR-26	9.0	+182	0.09	6.32	670	743	0.37	1.03	0	0	0
L20-06	HR-27	8.0	+274	0.07	6.05	632	697	0.85	2.72	0	0	0
C9-02	HR-21	8.0	+240	0.07	6.47	651	679	1.42	2.50	62	22	84
L17-02	HR-22	8.0	+198	0.07	6.42	574	654	2.02	3.08	44	41	85
L7-02	HR-23	8.0	+215	0.07	6.03	490	531	0.24	2.44	38	54	92
C10-02	HR-24	7.0	+221	0.07	5.26	651	706	6.35	9.25	14	0	14
C3-02	HR-25	8.0	+240	0.07	6.34	632	668	16.72	19.74	9	4	13
C19-02	HR-30		Test in 289°C Air			888	894	6.41	10.21	1	0	1
C19-04	HR-31	8.0	+252	0.07	6.18	750	769	6.06	8.79	1	0	1
L6-02	HR-32	8.0	+250	0.07	6.40	502	546	2.45	3.77	8	27	35
L14-02	HR-33	8.0	+246	0.08	6.07	760	703	1.90	4.67	84	2	86
L13-02	HR-34	7.0	+222	0.09	6.85	602	624	1.67	4.95	55	2	57
C04-02	HR-35	7.0	+259	0.08	6.54	634	680	1.07	2.02	-	-	-
L05-02	HR-36	7.0	+243	0.07	6.85	665	725	3.07	4.57	-	-	-

[a]Tested at 289°C at strain rate of 1.65×10^{-7} s^{-1} in simulated BWR water containing ≈ 8 ppm DO.

Table 5. Composition of model austenitic SSs irradiated to fluence of ≈0.9 x 10²¹ n·cm⁻² (E > 1 MeV) and results of SSRT tests^a and SEM fractography

Alloy ID	Composition (wt.%)								Mo/Nb	Remarks[b]	YS (MPa)	UTS (MPa)	UE (%)	TE (%)	TGSCC (%)	IGSCC (%)	TG+IGSCC (%)
	Ni	Si	P	S	Mn	C	N	Cr									
L22-02	13.30	0.024	0.015	0.004	0.40	0.003	0.001	16.10	Mo 2.04	HP 316L: Low Si, N	475	549	4.20	5.82	30	35	65
L11-02	8.15	0.47	0.097	0.009	1.02	0.014	0.004	17.40	-	high P; low Si, C, S, N	820	856	0.43	1.65	50	14	64
L18-02	8.13	0.14	0.016	0.033	1.13	0.080	0.001	18.00	-	low Si, N	710	755	3.98	5.05	38	14	52
L20-05	8.91	0.017	0.010	0.004	0.41	0.002	0.002	18.10	O 0.0940	HP 304L: low Si, N, Mn	670	743	0.37	1.03	0	0	0
L20-06	8.91	0.017	0.010	0.004	0.41	0.002	0.002	18.10	O 0.0940	HP 304L: low Si, N, Mn	632	697	0.85	2.72	0	0	0
C9-02	8.75	0.39	0.013	0.013	1.72	0.062	0.065	18.48	-	low Si; high Mn	651	679	1.42	2.50	62	22	84
L17-02	8.00	0.66	0.090	0.009	0.48	0.061	0.078	15.30	O 0.0090	high P; low Cr, Mn, S	574	654	2.02	3.08	44	41	85
L7-02	10.60	0.18	0.040	0.038	1.02	0.007	0.111	15.40	O 0.0274	high N, O; low Si, C	490	531	0.24	2.44	38	54	92
C10-02	8.13	0.55	0.033	0.002	1.00	0.060	0.086	18.19	-	CP 304: low S; high N	651	706	6.35	9.25	14	0	14
C3-02	8.91	0.46	0.019	0.004	1.81	0.016	0.083	18.55	-	CP 304L: high Mn, N; low S	632	668	16.72	19.74	9	4	13
C19-04	8.08	0.45	0.031	0.003	0.99	0.060	0.070	18.21	O 0.0200	CP 304: low S	750	769	6.06	8.79	1	0	1
L6-02	10.00	1.90	0.020	0.005	1.13	0.096	0.087	17.10	O 0.0058	high Ni, Si	502	546	2.45	3.77	8	27	35
L14-02	7.93	1.49	0.080	0.002	1.76	0.107	0.028	15.00	O 0.0045	high Si, P, Mn; low Cr, S	703	760	1.90	4.67	84	2	86
L13-02	8.08	1.18	0.027	0.022	0.36	0.026	0.001	17.40	-	high Si, S; low Mn, C, N	602	624	1.67	4.95	55	2	57
L04-02	10.20	0.94	0.031	0.010	1.75	0.110	0.002	15.80	-	high Ni, Si, C; low N, Cr	634	680	1.07	2.02	-	-	-
L05-02	9.66	0.90	0.113	0.028	0.47	0.006	0.033	21.00	-	high Si, P, Cr; low Mn, C	665	725	3.07	4.57	-	-	-

[a] Tested at 289°C at strain rate of 1.65×10^{-7} s^{-1} in simulated BWR water containing ≈8 ppm DO.
[b] HP = High purity; CP = Commercial purity.
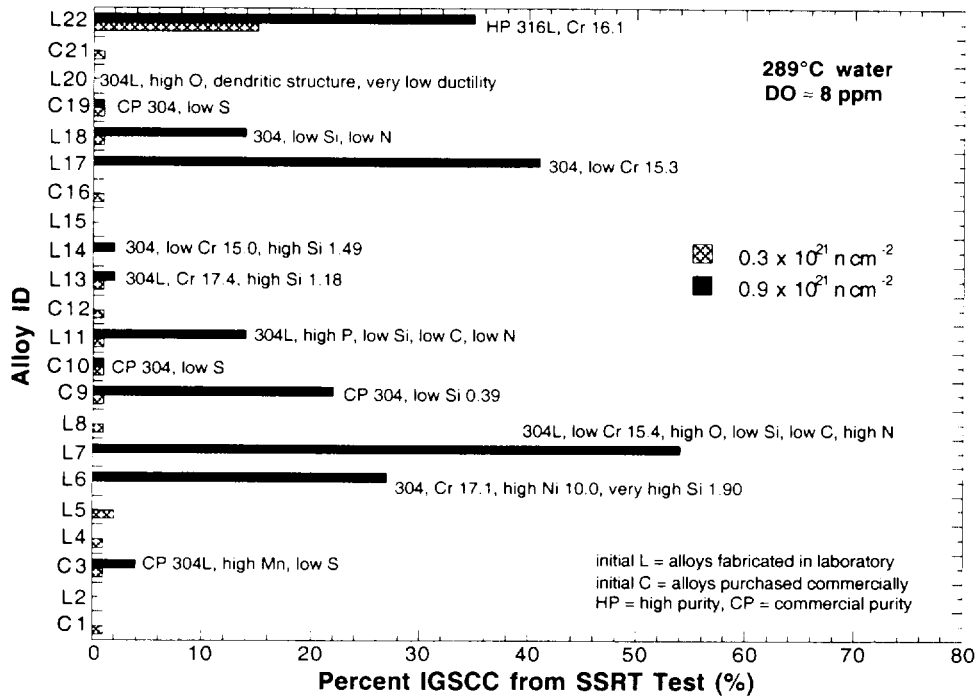
Figure 8. Percent IGSCC of fracture surfaces of model austenitic SS alloys tested after irradiation to ≈0.9 x 10⁻²¹ n·cm⁻² (E > 1 MeV) in the Halden reactor

Test results obtained from two specimens of a low-Cr Type 304 SS alloy, L4 (Cr ≈15.8 wt.%), and a high-Cr alloy, L5 (Cr ≈21 wt.%), provided insight into the effect of bulk

Cr concentration. After irradiation to $\approx 0.9 \times 10^{21}$ n·cm^{-2} (E > 1 MeV), the low-Cr alloy exhibited relatively low ductility (i.e., uniform elongation $\approx 1\%$, total elongation $\approx 2\%$, Table 4), whereas the high-Cr alloy L5 exhibited significantly higher ductility (i.e., uniform elongation $\approx 3\%$, total elongation $\approx 4.6\%$). The high-Cr alloy L5 also contains a relatively high concentration of Si (≈ 0.90 wt.%). The relatively good performance of the high-Cr alloy L5 was also manifested by the highest ductility among all the alloys irradiated to $\approx 0.3 \times 10^{21}$ n·cm^{-2} (E > 1 MeV).[66] Consistent with this, low-Cr Type 304 SS heats L17 (Cr 15.30 wt.%) and L7 (Cr 15.40 wt.%) exhibited significant susceptibilities to IASCC, and percent IGSCC ranging from 41 to 54, after irradiation to $\approx 0.9 \times 10^{21}$ n·cm^{-2} (E > 1 MeV). This finding indicates that high Cr concentration plays a major role in suppressing the susceptibility of steels to IASCC.

Results of SEM fractographic analysis showed that susceptibilities of high-Si Type 304 SS alloys L14 (Si 1.49 wt.%) and L13 (Si 1.18 wt.%) to IASCC were negligible after irradiation to $\approx 0.9 \times 10^{21}$ n·cm^{-2} (E > 1 MeV). In spite of a low Cr concentration (15 wt.%), the high-Si alloy L14 exhibited negligible susceptibility to IASCC; this appears to be related to the beneficial effect of high Si concentration; however, results from further investigations, especially SSRT tests on higher fluence specimens, are needed. Furthermore, excessively high Si concentration would not be desirable from the standpoint of phase stability, weld performance, and irradiation-induced precipitation. However, Alloy L6, which contains high concentrations of Ni (≈ 10 wt.%) and Si (≈ 1.9 wt.%), exhibited, significant IGSCC of $\approx 27\%$. This could be related to irradiation-enhanced formation of G-phase film on grain boundaries that could occur because of the unusually high concentrations of Ni and Si in the bulk material and subsequent segregation of Ni and Si to grain boundaries via an irradiation-induced process.

Of the four commercial alloys of Type 304 SS tested after irradiation to $\approx 0.9 \times 10^{21}$ n·cm^{-2} (E > 1 MeV), Alloys C10, C3, and C19 exhibited insignificant susceptibility to IGSCC (Fig. 8); all three alloys contained a low S concentrations of <0.004 wt.%. The composition of IASCC-resistant Heats C10 and C19 is virtually identical (Table 3). Effects of fluence on the stress–vs.–elongation of the IASCC-resistant heat C19, measured in water (≈ 8 ppm DO) and air at 289°C, are shown in Fig. 9. After irradiation to $\approx 0.9 \times 10^{21}$ n·cm^{-2} (E > 1 MeV), maximum strength of the material was somewhat lower in water than in air, i.e., ≈ 790 vs. ≈ 900 MPa. This could be attributed to the effect of H uptake in a water environment, which promotes dislocation slip in steels. However, in both environments, ductility was similar and percent IGSCC was negligible.

3.3 Stress Corrosion Cracking of Type 304 Stainless Steel Irradiated to Very High Dose in the EBR-II Reactor (H. M. Chung, W. E. Ruther, and R. V. Strain)

3.3.1 Introduction

As in the present investigation on the Halden-reactor-irradiated SSs, irradiation–induced grain–boundary depletion of Cr has been considered by most investigators to be the primary metallurgical process that causes IASCC at relatively low damage levels (e.g., ≈ 1-10 dpa). Very narrow Cr–depleted zones at grain boundaries have been observed by field-emission-gun analytical electron microscopy[43,44,49,50] and Auger electron spectroscopy.[41,44,45,59] Furthermore, the results of electrochemical potentiokinetic reactivation tests[36] and the effects of ECP[39,41] and DO[40,41] on susceptibility of nonirradiated, thermally sensitized material (where Cr depletion is widely recognized as the primary factor) to IGSCC and on susceptibility
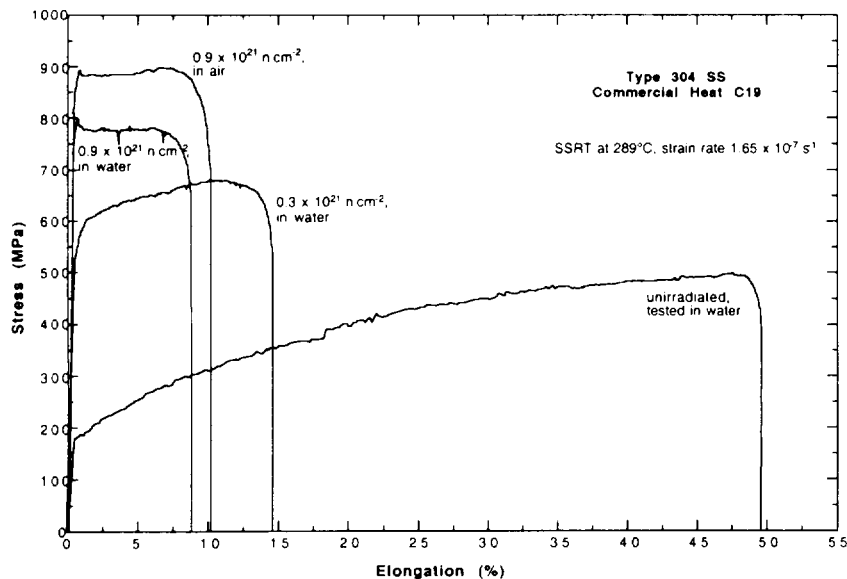
Figure 9.
Effects of
environment and
fluence on stress vs.
elongation of IASCC-
resistant Heat C19 of
Type 304 SS.

of BWR–irradiated solution–annealed material to IASCC during SSRT tests[39-41] are reported to be similar.

However, contrary to expectations based on the strong effect of ECP on SCC associated with grain-boundary Cr depletion, IG cracking of highly stressed components has been reported in PWRs[32,33,51] (which operate at low ECPs), and the susceptibility of PWR–irradiated components[35] or specimens[60] to IG cracking at low ECP has been observed in hot–cell experiments.[35,60] In the experiment of Manahan et al.,[35] 10%-cold-worked Type 304 SS specimens were tested in Ar at ≈315°C after irradiation to ≈7 dpa in a PWR. Although the authors considered that these specimens contained IG-type brittle-fracture morphology on as much as ≈35% of the fracture surfaces, the high-magnification fractographs do not clearly establish that the fracture surface morphology was true IG separation, especially when it is compared with IG cracking observed in control rod cladding in PWR water.[33,35] IG cracking in Ar gas or low-DO water has been reported by Hide et al.[58] for thermally sensitized Type 304 SS specimens irradiated to ≈0.4 dpa in water at ≈290°C in the Japan Material Testing Reactor and tested at ≈290°C. However, in that case, the IG crack morphology was limited to a very small fraction (< 5%) of the fracture surface near the specimen free surface, which should contain a high concentration of O (due to corrosion during irradiation).

If we consider this background, there does not appear to be strong evidence for the occurrence of IG cracking in inert gas or air in solution-annealed austenitic SSs for Type 304 SS irradiated up to ≈7 dpa at temperatures relevant to LWRs. However, as irradiation damage is increased to levels that can be expected by the end of design life (i.e., 20-100 dpa), significant microstructural evolution occurs. e.g., extensive Cr depletion and extensive segregation of Ni, Si, and other impurities on grain boundaries, and formation of dense defect clusters, microvoids, and irradiation-induced precipitates in grain matrices. The result is that, at very high dose, properties such as hardening, grain matrix deformation, grain-boundary amorphization could differ significantly from those of steels that have been exposed to relatively low doses of irradiation, and this could change the susceptibility to mechanical IG cracking and IGSCC.

Information about material behavior at high fluence is needed to help us to better understand the potential impact of irradiation on core internals such as BWR top guide and core plate and PWR baffle bolts. To this end, Type 304 SS specimens that had been fabricated from the hexagonal fuel can of the decommissioned EBR-II reactor after irradiation to ≈50 dpa at ≈370°C were tested in air and water. Posttest analyses were performed by SEM and TEM to elucidate the failure mechanism(s) at this high fluence. The initial tests were conducted at ≈289°C, and tests at ≈325°C in PWR-like water are planned.

3.3.2 Materials and Experimental Procedures

The geometry of the specimens for tensile and SSRT tests is shown in Fig. 10. The specimens (nominal wall thickness, 1 mm, or 0.040 in.) were machined in a hot cell from the hexagonal fuel can of the EBR-II reactor, which was decommissioned after more than 30 years of operation. The fuel can, fabricated from a commercial-grade solution-annealed Type 304 SS, was irradiated in liquid Na at ≈370°C to a fluence of ≈1.02 x 10^{23} n·cm^{-2} (E > 0.1 MeV), which corresponds to a damage level of ≈50 dpa. The average grain size of the as-irradiated specimens was ≈35 μm. Records of the composition of the archive ingot or the as-fabricated fuel can were not available. Before testing, the machined, irradiated specimens were first slightly polished to remove burrs and surface irregularities, and then, the final width and wall thickness of the specimen gauge section were measured at three locations.
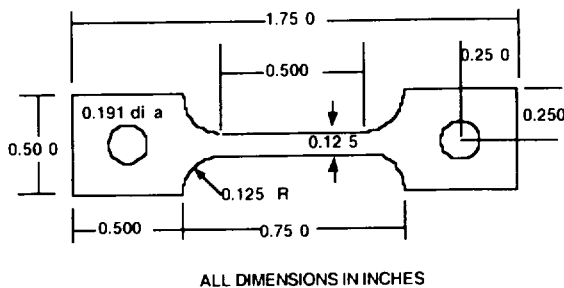
Figure 10.
Geometry of SSRT test specimens prepared from EBR-II reactor hexagonal fuel can.

ALL DIMENSIONS IN INCHES

Tensile properties and susceptibility to IG cracking were determined by SSRT tests on the specimens at 289°C in air and in water at a strain rate of 2.5 x 10^{-7} s^{-1}. All tests in water were conducted at 289°C in deionized high-purity water that contained ≈8 or ≈0.01 ppm DO. Concentration of DO, controlled by purging the deaerated water with an N/O mixture, was measured on the effluent side. Electrochemical potential was measured at the effluent side at regular intervals.

Posttest fractographic analysis was conducted by SEM to measure the percentage of ductile, transgranular, and IG fracture surface. One or two disks were carefully cut out of the fracture tips (≈1.5-2.0 mm away from the fracture surface) of the failed specimen. Thin-foil TEM specimens were jet-polished at room temperature in a solution of 25 mL of perchloric acid, 225 mL of acetic acid, and 50 mL of butylcellosolve. Analysis by TEM was performed at 100 keV in a JEOL 100-CXII scanning transmission electron microscope (STEM).

3.3.3 Results

Feedwater chemistry (i.e., DO, ECP, conductivity, and pH) and results from SSRT tests (i.e., 0.2%-offset yield strength, maximum strength, uniform strain, and total strain) are

summarized in Table 6. Also shown in Table 6 are the results of SEM fractographic analysis (i.e., ductile, IG, and TG fracture surface morphology) of the failed specimens. Figure 11 shows engineering stress vs. elongation of the specimens that were tested in air and water.

Table 6. SSRT test results for Type 304 SS specimens[a] from decommissioned EBR-II reactor hexagonal fuel can[b]

Spec. ID No.	α–γ Hot–Cell ID No.	SSRT[c] Test No.	Feedwater Chemistry				SSRT Parameters				Fracture Surface Morphology
			Oxygen Conc. (ppm)	Average ECP (mV SHE)	Cond. at 25°C (μS·cm^{-1})	pH at 25°C	Yield Stress (MPa)	Max. Stress (MPa)	Uniform Strain. (%)	Total Strain. (%)	
A-1	521-A	IR-96-10	Tested in Air				680	776	3.54	4.82	Ductile
E-1	521-C	IR-96-9	8.0	+210	0.061	6.87	Specimen fractured across shoulder				
B-1	521-B	IR-96-11	8.0	+202	0.067	7.10	447	472	0.47	2.41	90% IGSCC
F-1	521-D	IR-96-12	0.01	-318	0.065	6.71	602	664	0.68	2.12	Channel Fract.

[a]Specimen size 44.5 x 12.7 x 1.0 mm, gage section 12.7 x 3.2 x 1.0 mm
[b]Discharged after irradiation to ≈50 dpa (fluence 1.1 x 10^{23} n·cm^{-2}, E > 0.1 MeV) in sodium at ≈370°C
[c]Test at 289°C at a strain rate of 2.5 x 10^{-7} s^{-1} in deionized high-purity water or air
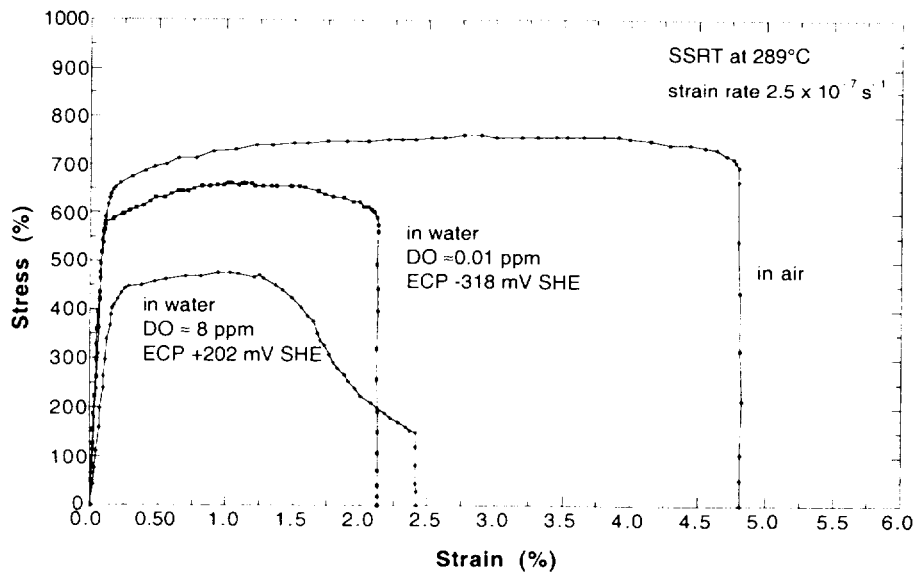
Figure 11. Engineering stress vs. strain of Type 304 SS from hexagonal fuel assembly can irradiated in EBR-II to ≈50 dpa at ≈370°C and tested at 289°C in air and high-purity water

3.3.3.1   Deformation and Failure Behavior in Air

The highly irradiated steel exhibited good work-hardening capability and surprisingly high ductility in air, manifested by uniform and total elongations as high as ≈3.5 and ≈4.8%, respectively. Tensile properties of the ≈50-dpa material are shown in Fig. 12, with similar data reported for commercial-grade Type 304 SSs that were irradiated to <5 dpa and tested in BWR-like conditions. Strength of the EBR-II material at ≈50 dpa was significantly lower than that of BWR components at < 5 dpa that were tested under similar conditions, i.e., ≈680 vs. ≈850 MPa yield strength and ≈780 vs. ≈900 MPa ultimate tensile strength, respectively. This difference is most likely due to the fact that irradiation temperature of the former material was significantly higher than that of the latter (i.e., ≈290 vs. ≈370°C).
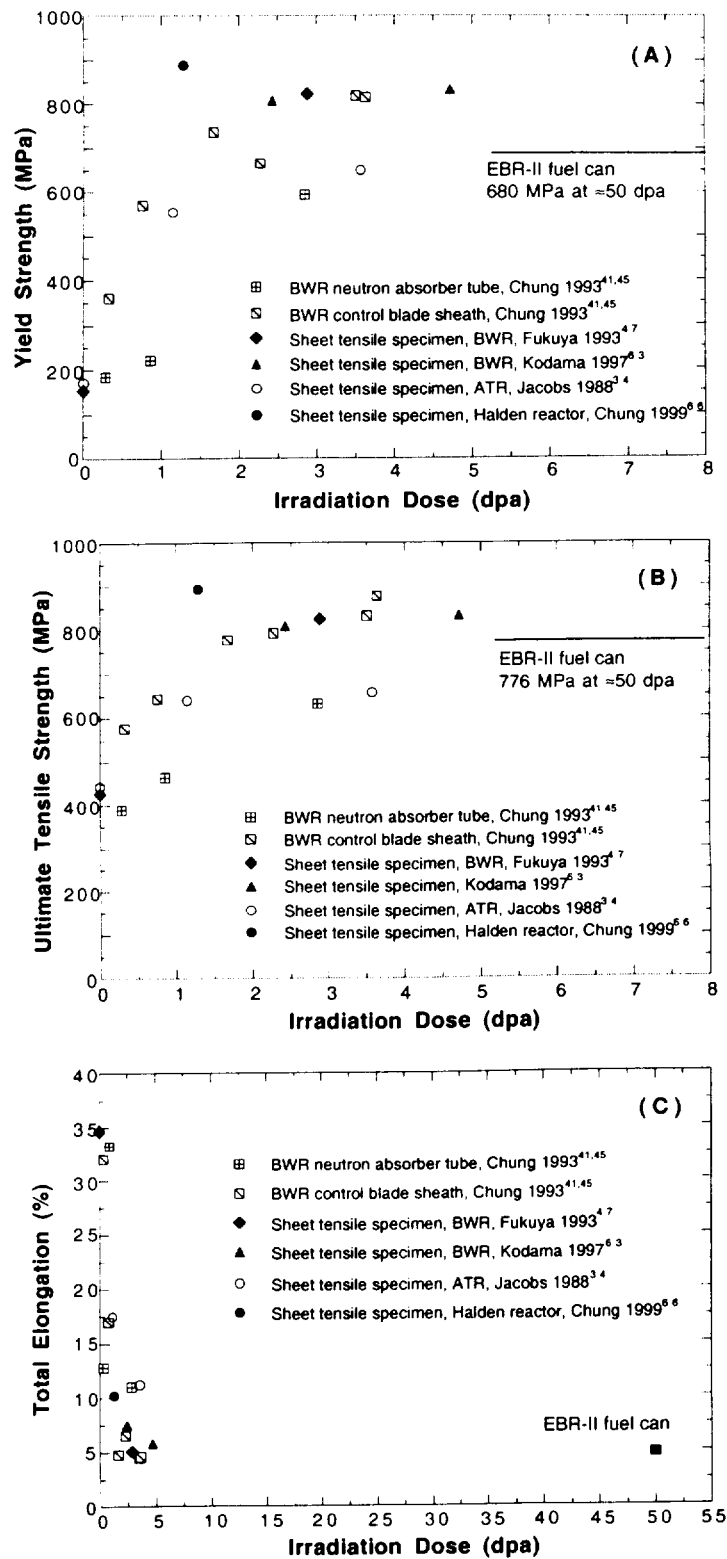
Figure 12. Comparison of (A) yield strength, (B) ultimate tensile strength, and (C) total elongation vs. irradiation dose for EBR-II fuel can, irradiated at ≈370°C to ≈50 dpa and tested in air at 289°C, and similar data for solution-annealed commercial-grade Type 304 SS irradiated in BWR and tested at ≈289°C

Fracture surface morphology of the air-tested specimen was entirely ductile (Fig. 13); no evidence of IG separation was observed in any part of the fracture surface. Many dislocation loops and microvoids were observed in the material; however, there was no evidence that microvoids, typically ≈20-60 nm in size, aggregated on grain boundaries (Fig. 14). This finding is consistent with the observation that the material did not fail by IG separation in air.
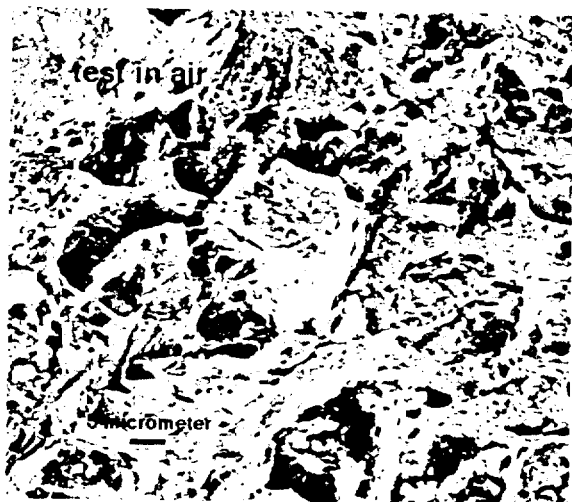
Figure 13.
SEM fractograph of ≈50-dpa Type 304 SS specimen irradiated in EBR-II reactor and tested in air at ≈289°C
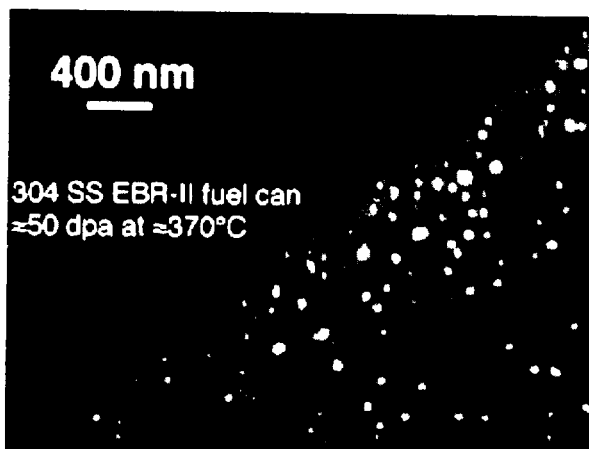
Figure 14.
Bright-field TEM image showing void distribution near grain boundary of ≈50-dpa Type 304 SS specimen irradiated in EBR-II reactor.
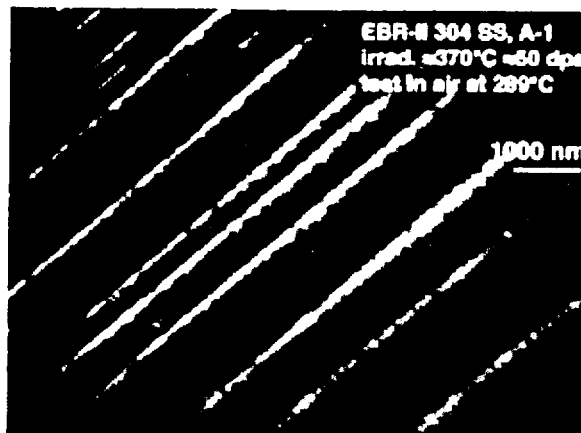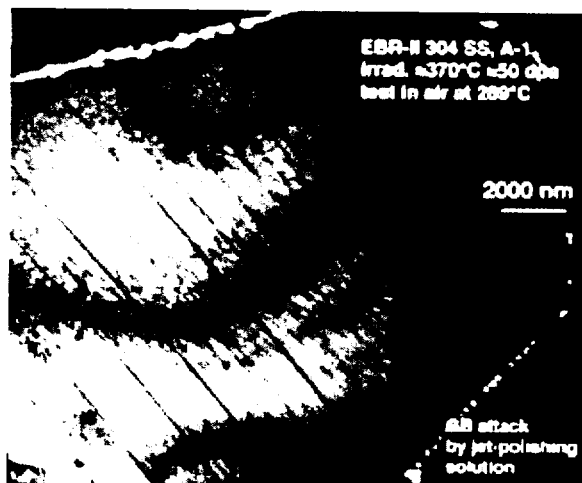
Figure 15. Twins in fracture tip of ≈50-dpa specimen tested in air: (left) bright-field image and (right) dark-field image produced with a twin reflection.

Results of TEM characterization of the thin-foil specimen, cut out of the gauge section adjacent to the fracture surface, showed that twinning was the predominant deformation mechanism (Fig. 15). Twinned grains exhibited characteristic twin reflections in selected area diffraction patterns (SADs), and clear dark-field images of (111) twins could be obtained by using the twin reflections (Fig. 15).

3.3.3.2 Failure Behavior in High-ECP Water

In contrast to the deformation behavior in air, in an oxidizing environment of the high-ECP water (ECP +202 mV SHE, DO ≈8 ppm), the material exhibited negligible work-hardening capability and poor ductility, as evidenced by low uniform and total elongations of only ≈0.5 and ≈2.4%, respectively. Deformation steps on specimen side surfaces were absent. The material exhibited high susceptibility to IGSCC (Fig. 16) as indicated by an IG fracture surface morphology as high as ≈90% in one test and brittle cracking near the shoulder-region hole in another.
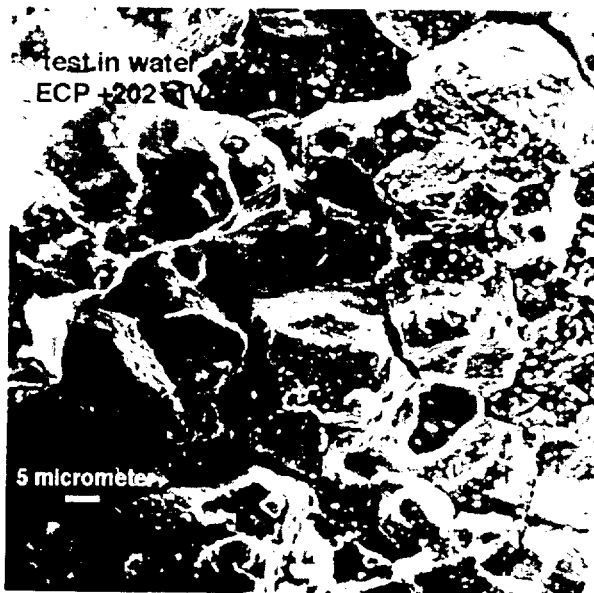
Figure 16.
SEM fractograph of ≈50-dpa Type 304 SS specimen irradiated in EBR-II reactor and tested in water at ≈289°C. DO ≈8 ppm. ECP ≈+202 mV SHE

3.3.3.3 Failure Behavior in Low-ECP Water

In the low-ECP water (ECP –318 mV SHE, DO ≈0.01 ppm), the material exhibited low work-hardening capability and poor ductility (uniform and total elongations ≈0.7 and ≈2.1%, respectively). However, despite the poor ductility, the percent IGSCC was negligible, and the fracture surface of the specimen was essentially ductile (Fig. 17). No evidence of IG separation was observed, showing that low levels of DO and ECP were effective in suppressing the susceptibility of the heavily irradiated material to IGSCC. The free side surface of the fracture tip was characterized by high-density deformation steps, indicating that localized deformation occurred in the low-ECP water.

Despite negligible susceptibility to IGSCC, ductility of the material was significantly lower in low-ECP water (–318 mV SHE) than in air (i.e., total elongation was 2.1% in water vs. 4.8% in air). Because this behavior is indicative of differing types of deformation mechanisms that may operate in air and in low-ECP water, TEM analysis was conducted on disk specimens that
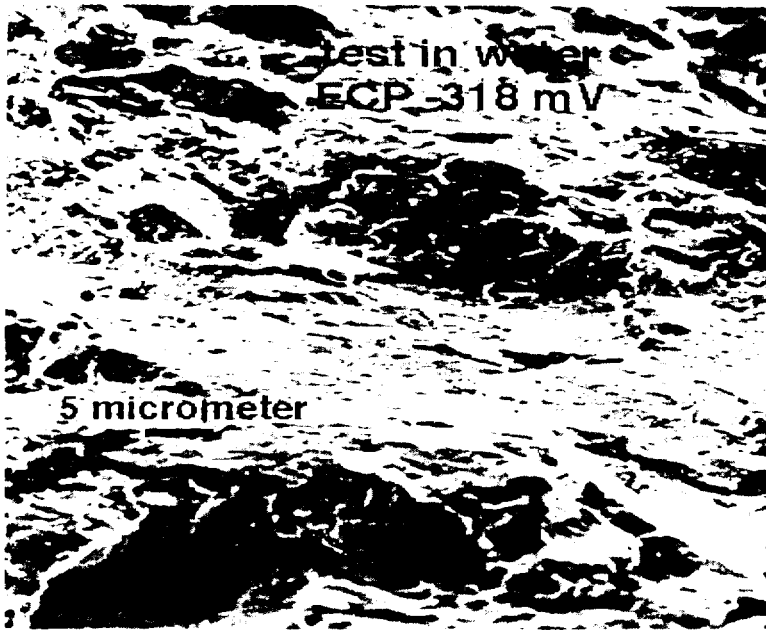
Figure 17.
SEM fractograph of ≈50-dpa Type 304 SS specimen irradiated in EBR-II reactor and tested in water at ≈289°C, DO ≈0.01 ppm, ECP ≈-318 mV SHE

were carefully excised from the fracture tips of the specimens. The primary deformation mode in the fracture tip in the low-ECP water was dislocation channeling (Fig. 18), which is in contrast to the observation that the primary deformation mode of the material in air was twinning. In the highly stressed and deformed fracture tip in the low-ECP specimen, twinning was negligible. Twins and dislocation channels exhibit diffraction behavior and dark-field-imaging characteristics that differ distinctively. Deformation mode away from the fracture tip was, however, not examined.

In addition to dense dislocation loops and microvoids, the highly irradiated material contained dense irradiation-induced precipitates. These dense precipitates were present in all specimens, showing that they did not precipitate during the tests. Dark-field images showed that short line dislocations were frequently "decorated" with precipitates. Although the precipitates could not be identified conclusively at this time, they were cleared in dislocation channels (Fig. 18 D). Grain-boundary offsets were also observed (Fig. 18 A).

3.3.4 Discussion

Results from these experiments show that despite the very high dose level, IG failure did not occur in the EBR-II-irradiated steel in air or in low-ECP water. However, similar to Type 304 SS components or specimens irradiated to ≈2-5 dpa in BWRs, the EBR-II-irradiated steel exhibited extensive susceptibility to IGSCC in high-ECP oxidizing water. Furthermore, as shown in Fig. 19, the effects of ECP and DO on the susceptibility of the ≈50-dpa material to IGSCC are similar to those obsrved in tests on Type 304 SS BWR core internal components. This observation indicates that the stress corrosion process associated with irradiation-induced grain-boundary Cr depletion plays the primary role in BWR-like oxidizing water.

Obviously, the results of this experiment do not support the premise that purely mechanical separation of grain boundaries occurs or is likely to occur in water at very high irradiation doses. The results also indicate that if sufficiently low levels of ECP can be
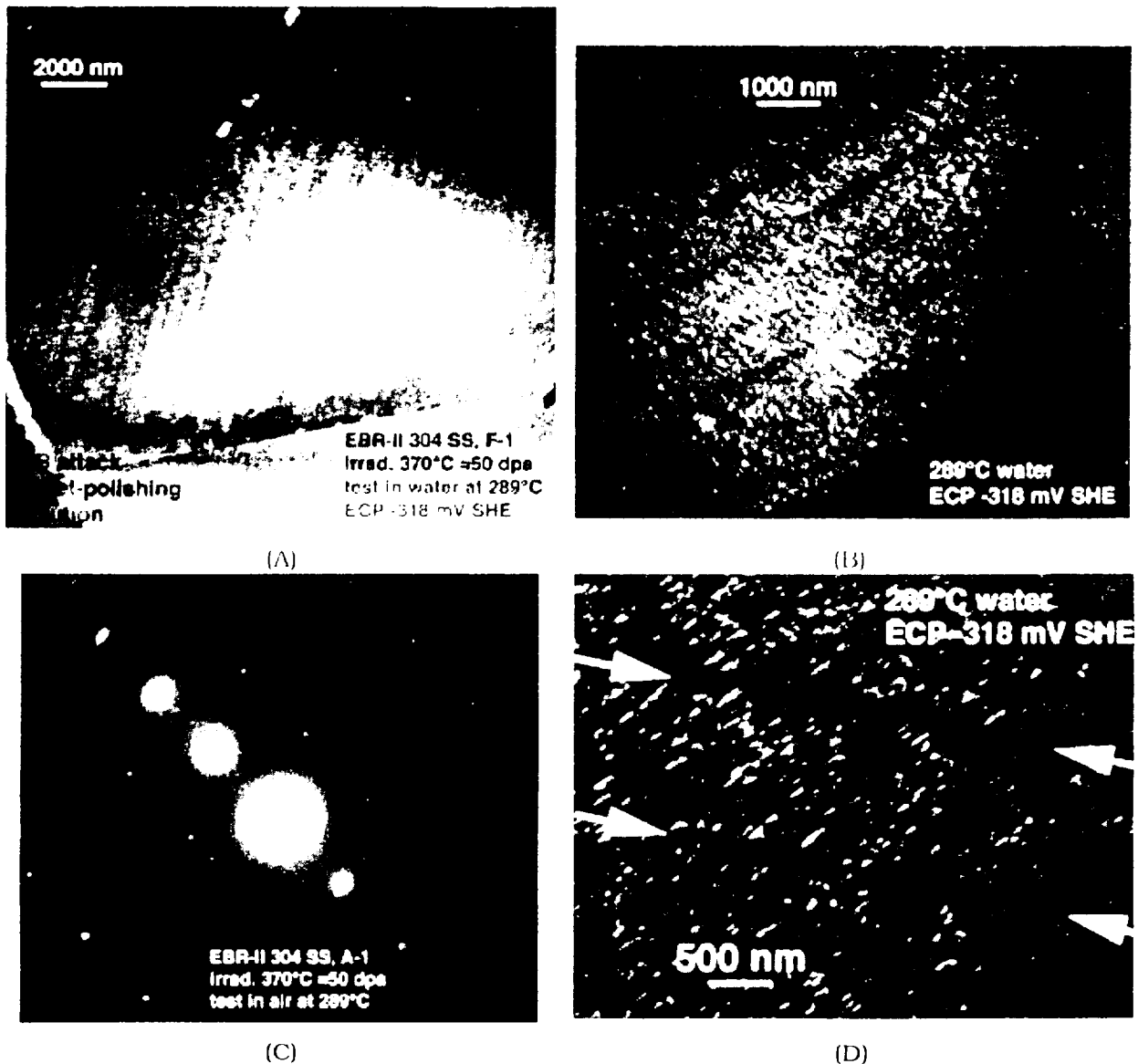
Figure 18. Microstructure of fracture tip of specimen tested in water, ECP -318 mV: (A) bright-field image showing dislocation channels and grain-boundary offset, (B) high-magnification bright-field image of channels, (C) selected area diffraction pattern showing reflections from unidentified precipitates, and (D) dark-field image from a precipitate reflection showing that dislocation channels are cleared of precipitates

maintained, susceptibility to IASCC could potentially be suppressed by use of proper water chemistry even at the end of life, at least under BWR-like conditions at ≈290°C.

It is not clear why dislocation channeling is promoted, and, at the same time, twinning is suppressed in low-ECP water. However, one possible explanation is that a significant number of H atoms penetrated into the relatively highly stressed fracture tip region during the test in the low-ECP water; such a penetration of H atoms promotes dislocation slip in the region before the critical stress required to trigger twinning is reached. It is likely that, as suggested by Bruemmer et al.,[46] twins are nucleated only when stress in a grain matrix is sufficiently high and reaches a critical stress. If dislocation channeling is promoted, as in low-ECP water,
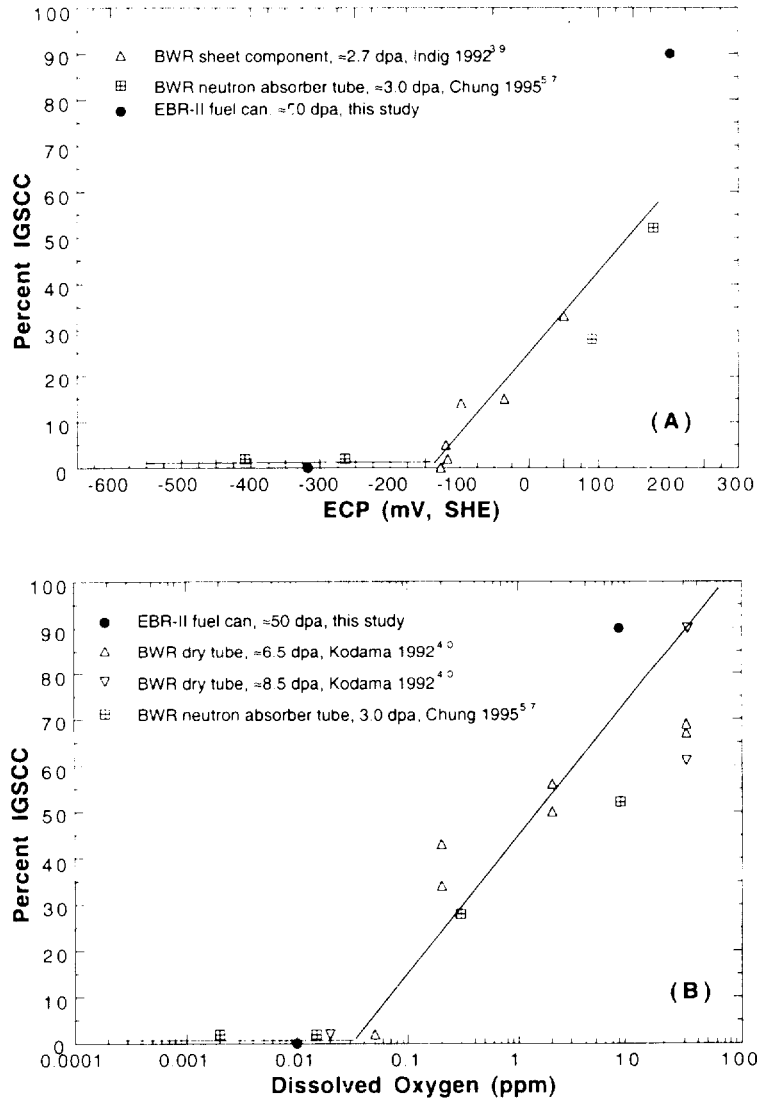
Figure 19. Susceptibility to IGSCC (in percent IGSCC) vs. ECP (A) and DO (B) of commercial-grade Type 304 SS BWR components and EBR-II fuel can.

strain hardening will be limited to the dislocation channels or to the immediate vicinity of the channels; hence, it will be more difficult for a grain matrix as a whole to reach the critical stress required to trigger twinning. This premise, then, implies that at very high levels of irradiation, some factor related to the presence of low-ECP water (e.g., H uptake) promotes dislocation channeling in the fracture tip, thereby leading to limited ductility in the material. Furthermore, the observation that the very fine irradiation-induced precipitates were swept by dislocation channels (Fig. 18 D) indicates that dense precipitates, rather than "black-dot" defects or defect clusters, were the primary barriers that were "pushed-out" or sheared by moving dislocations, inducing dislocation channeling. Formation of black-dot defects or defect clusters, commonly produced in high density under LWR irradiation conditions, was insignificant in the EBR-II component, probably because of the relatively higher irradiation temperature of $\approx 370°C$ of the latter material.

3.3.5 Conclusions

Slow-strain-rate tests at 289°C and posttest microstructural examination were conducted on material from a Type 304 SS hexagonal fuel can that was irradiated to ≈50 dpa at ≈370°C in the EBR-II reactor. Although the irradiation conditions are not completely prototypical, the material represents a limiting end-of-life fluence for BWR internal components. Major observations and findings are as follows:

- No IG failures were observed in tests in air at 289°C. This finding suggests that IG failures cannot occur by purely mechanical processes, even at ≈50 dpa.

- As in the case of BWR internal components irradiated to 2–5 dpa, IG failures were not observed in tests in water at low ECPs. However, virtually complete IG failure was observed in tests in water at high ECPs. These results are consistent with the premise that irradiation-induced grain-boundary Cr depletion plays a major role in IASCC.

- In the tests in air, extensive twinning leads to relatively high tensile ductilities in Type 304 SS at 289°C, even at ≈50 dpa.

- In low-ECP water at 289°C, tensile ductilities were low, in spite of the fact that IG failures were not observed. The twinning observed in the air tests was negligible in the fracture region, and dislocation channeling was the primary process for deformation and failure in the low-ECP water. Dense irradiation-induced precipitation and the presence of the low-ECP water appear to play important roles in dislocation channeling.

3.4 Fracture Toughness J–R Test of Austenitic Stainless Steels Irradiated in the Halden Reactor (E. E. Gruber and O. K. Chopra)

Austenitic SSs are used extensively as structural alloys in reactor pressure vessel internal components because of their high strength, ductility, and fracture toughness. Fracture of these steels occurs by stable tearing at stresses well above the yield stress, and tearing instabilities require extensive plastic deformation. However, exposure to high levels of neutron irradiation for extended periods changes the microstructure and degrades the fracture properties of these steels. Irradiation leads to a significant increase in yield strength and reduction in ductility and fracture resistance of austenitic SSs.[67-69]

Neutron irradiation of austenitic SSs at temperatures below 400°C leads to the formation of a substructure with very fine defects that consist of small (<5-nm) vacancy and interstitial loops or "black spots" and larger (>5-nm) faulted interstitial loops.[70-72] The latter are obstacles to dislocation motion, and lead to matrix strengthening and increase in tensile strength. Also, irradiation-induced defects cause loss of ductility and reduced strain-hardening capacity of the material. The effects of radiation on various austenitic SSs vary significantly and appear to be related to minor differences in steel composition, which can influence the stacking fault energy and/or irradiation-induced microstructure. As the yield strength approaches ultimate strength, planar slip or dislocation channeling is promoted and leads to pronounced degradation in the fracture resistance of these steels.[69] In general, higher stacking-fault energy enhances and cold working inhibits dislocation channeling.

The effect of neutron exposure on the fracture toughness J_{Ic} of austenitic SSs irradiated at 350–450°C is shown in Fig. 20.[73-81] The effects of irradiation may be divided into three regimes: little or no loss of toughness below a threshold exposure of ≈1 dpa, substantial decrease in toughness at exposures of 1–10 dpa, and no effect on toughness above a saturation exposure of 10 dpa. The effect is largest in high–toughness steels. The degradation in fracture properties saturates at a J_{Ic} value of ≈30 kJ/m^2 (or equivalent critical stress intensity factor K_{Jc} of 70 MPa m$^{0.5}$). Also, the failure mechanism changes from dimple fracture to channel fracture.

Most of the existing fracture toughness test data have been obtained at temperatures above 350°C; fracture toughness results that are relevant to LWRs are very limited.[68] This report presents fracture toughness J–R curves for four heats of Type 304 SS that were irradiated to fluence levels of ≈0.3 and 0.9 x 10^{21} n·cm^{-2} (E > 1 MeV) (≈0.45 and 1.35 dpa) at ≈288°C in a He environment in the Halden boiling heavy water reactor. The results are compared with data obtained from irradiated reactor internal components removed from operating plants.
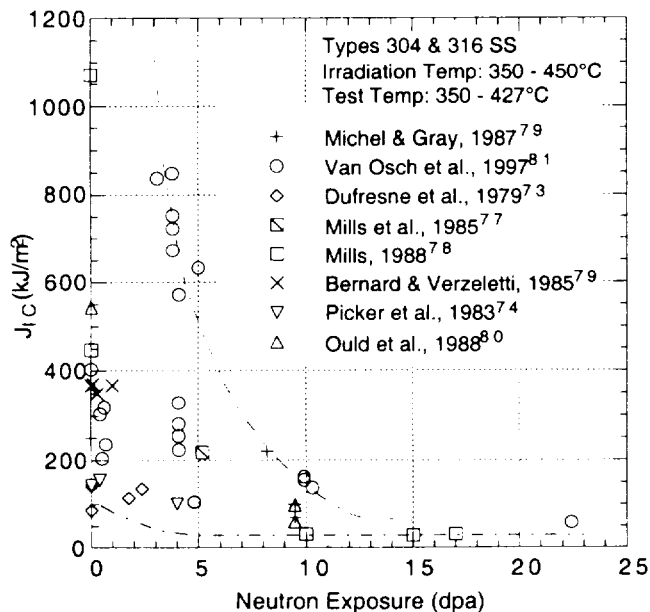
Figure 20.
Fracture toughness J_{IC} of austenitic Types 304 and 316 SS as a function of neutron exposure

3.4.1 Experimental

Fracture toughness J–R curve tests were performed on 1/4–T CT specimens in air at 288°C according to the requirements of ASTM Specification E 1737 for J–Integral Characterization of Fracture Toughness. Crack extensions were determined by both DC potential and elastic unloading compliance techniques. The composition of the various heats of Type 304 SS is presented in Table 7. Figure 21 shows the configuration of the CT specimens. Calculations of crack length and J–integral were performed with the correlations recommended for disk–shaped CT specimens in ASTM Specification E 1737.

The fracture toughness test facility at ANL is designed for in–cell testing, with the hydraulic actuator, test train, furnace, and other required equipment mounted on top of a

Table 7. *Composition (wt.%) of Type 304 SS alloys irradiated in the Halden Reactor*

Alloy ID[a]	Vendor Heat ID	Analysis	Ni	Si	P	S	Mn	C	N	Cr	O[b]
L2	BPC-4-111	Vendor	10.50	0.82	0.080	0.034	1.58	0.074	0.102	17.02	66
		ANL									
C16	PNL-SS-14	Vendor	12.90	0.38	0.014	0.002	1.66	0.020	0.011	16.92	–
		ANL	12.32	0.42	0.026	0.003	1.65	0.029	0.011	16.91	157
C19	DAN-74827	Vendor	8.08	0.45	0.031	0.003	0.99	0.060	0.070	18.21	–
		ANL	8.13	0.51	0.028	0.008	1.00	0.060	0.068	18.05	200
L20	BPC-4-101	Vendor	8.91	0.17	0.010	0.004	0.41	0.002	0.002	18.10	–
		ANL	8.88	0.10	0.020	0.005	0.47	0.009	0.036	18.06	940

[a]First letters "C" and "L" denote commercial and laboratory heats, respectively.
[b]In wppm.
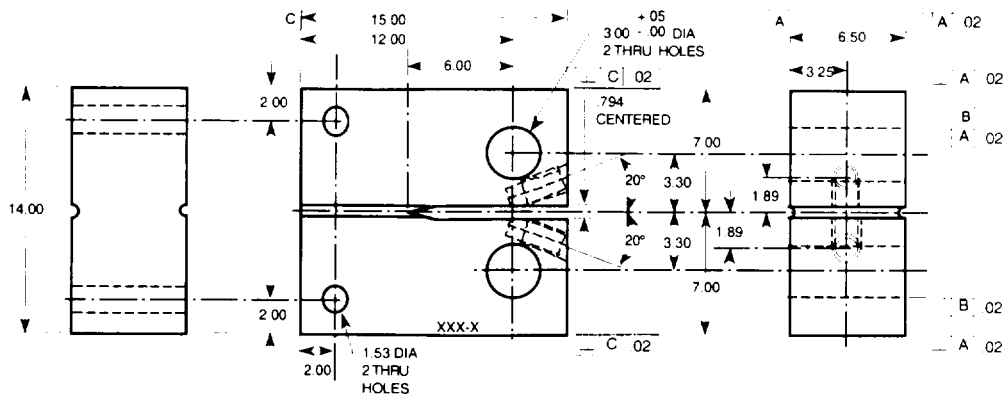
Figure 21. *Configuration of compact-tension specimen for this study. Dimensions in mm.*

portable, wheeled cart that can be easily rolled into the cell. Detailed descriptions of the test facility and procedures have been presented elsewhere.[82-84]

Before testing, the specimens were fatigue-precracked at room temperature. The precracked specimens were then tested at 288°C at a constant extension rate; tests were interrupted periodically to determine crack length. Specimens were held at constant extension to measure crack length by both the DC-potential-drop and elastic unloading compliance techniques. For most steels, load relaxation occurs during the hold period or unloading, which causes a time-dependent nonlinearity in the unloading curve. Consequently, before unloading, the specimen was held for ≈1 min to allow load relaxation.

Specimen extension was monitored and controlled outside of the high-temperature zone. The displacement of load points (center of the loading pins) was determined by subtracting the machine compliance from the measured extension.

The final crack size was marked by heat tinting and/or by fatigue cycling at room temperature. The specimens were then fractured and the initial (i.e., fatigue precrack) and final (test) crack lengths of both halves of the fractured specimen were measured optically. The crack lengths were determined by the 9/8-averaging technique, i.e., the two near-surface measurements were averaged and the resultant value was averaged with the remaining seven measurements.

The crack length measurements obtained by the elastic unloading compliance method were adjusted only with the measured initial crack length, whereas those obtained by the DC-potential-drop technique were adjusted with both the initial and final crack lengths. The two-point pinning method was used to correct the measured potentials. The DC-potential data were also corrected for the effects of plasticity on the measured potential, i.e., large crack-tip plasticity can increase measured potentials without crack extension because of resistivity increases. As per ASTM E 1737, the change in potential before crack initiation was ignored and the remainder of the potential change was used to establish the J-R curve. Plots of normalized potential vs. loadline displacement generally remain linear until the onset of crack extension. For all data within the linear portion of the curve, crack extension was calculated from the blunting-line relationship $\Delta a = J/(4\sigma_f)$. For high-strain-hardening materials, e.g., austenitic SSs, a slope that is four times the flow stress $(4\sigma_f)$ represents the blunting line better than a slope of $2\sigma_f$, as defined in ASTM E 1737.[69]

3.4.2 Results

3.4.2.1 Nonirradiated Type 304 Stainless Steel

Fracture toughness J-R curve tests on nonirradiated specimens were conducted on only one of the model austenitic SS alloys, i.e., Heat L2. The load-vs.-loadline displacement and fracture toughness J-R curves for the material are shown in Figs. 22 and 23, respectively. The curve obtained by the unloading compliance method shows good agreement with that obtained by the DC-potential method. However, the fracture toughness of Heat L2 is poor. The J-R curve is significantly lower than that observed for Type 304 SSs, Fig. 24.[78,85-87] For wrought austenitic SSs, the J_{ic} values at temperatures up to 550°C are typically >400 kJ/m²;[69] experimental J_{ic} for Heat L2 is ≈210 kJ/m². Fracture toughness J-R curve tests are in progress on nonirradiated Heats C16, C19, and L20.

3.4.2.2 Irradiated Type 304 Stainless Steels

Fracture toughness J-R curve tests were conducted at 288°C on Heats C19, L20, C16, and L2 of Type 304 SS irradiated in He at 288°C to 0.9 x 10^{21} n·cm^{-2} (E > 1 MeV) in the Halden reactor. Heats C19 and L20 were also tested after a fluence of 0.3 x 10^{21} n·cm^{-2} (E > 1 MeV). The load-vs.-loadline-displacement and fracture toughness J-R curves for the various steels are shown in Figs. 25-33. For all tests, the J-R curves obtained by the unloading-compliance method show very good agreement with those obtained by the DC-potential method.

Neutron irradiation at 288°C decreases the fracture toughness of all steels. Minor differences in the chemical composition of the steels, e.g., differences in Ni content for heats C16 and C19 or Si content for Heats L2 and L20, have little or no effect on the fracture toughness of irradiated steels. In general, fracture toughness of the Commercial Heats C16 and C19 is superior to that of the Laboratory Heats L20 and L2. The values of fracture toughness J_{ic} for the specimens irradiated to 0.9 x 10^{21} n·cm^{-2} are 326 and 331 kJ/m² for Heats C16 and C19, respectively, and 36 and 38 kJ/m² for Heats L2 and L20, respectively. Although J-R curve tests were conducted on only one of the heats in the nonirradiated
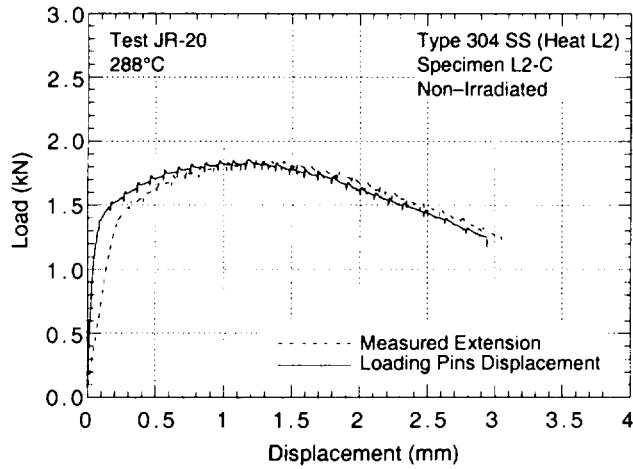
Figure 22.
Load vs. loadline displacement for nonirradiated Type 304 SS specimen of Heat L2 tested at 288°C
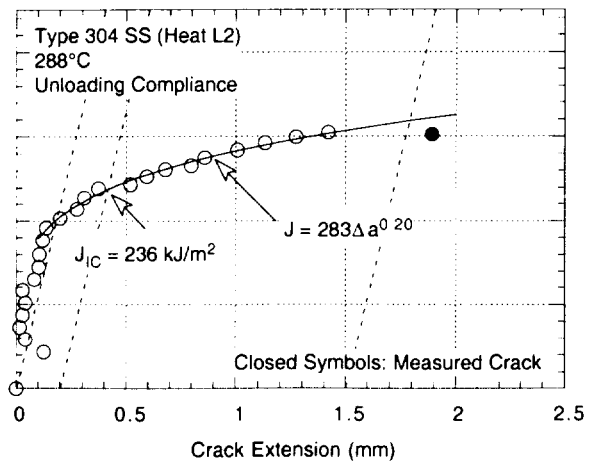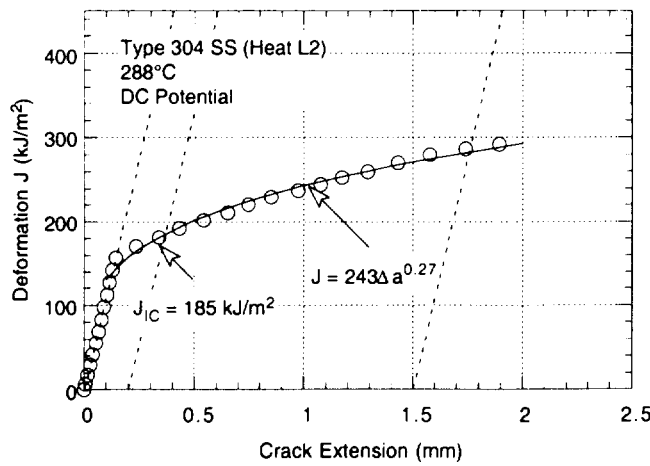
Figure 23. Fracture toughness J–R curve for nonirradiated Type 304 SS specimen of Heat L2 at 288°C, determined by DC–potential–drop and unloading compliance methods. Dashed lines represent the blunting line and 0.2– and 1.5–mm offset lines.
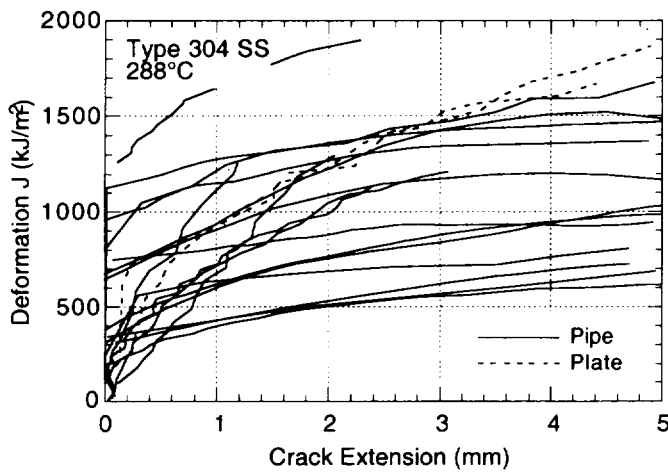
Figure 24.
Fracture toughness J–R curves for Type 304 SSs at 288°C
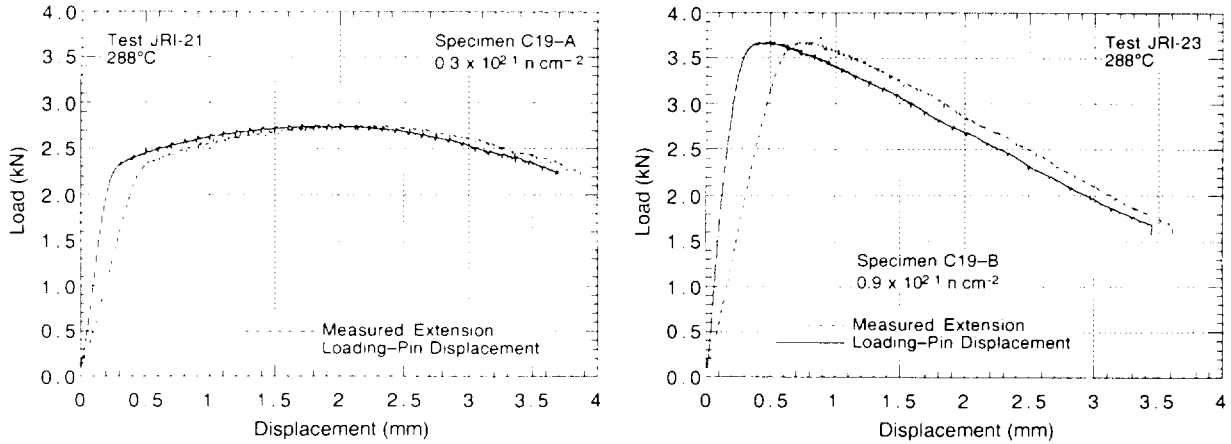
Figure 25. Load-vs.-loadline-displacement curves for Heat C19 of Type 304 SS irradiated to 0.3 and 0.9 x 10^{21} n·cm^{-2} in the Halden reactor at 288°C
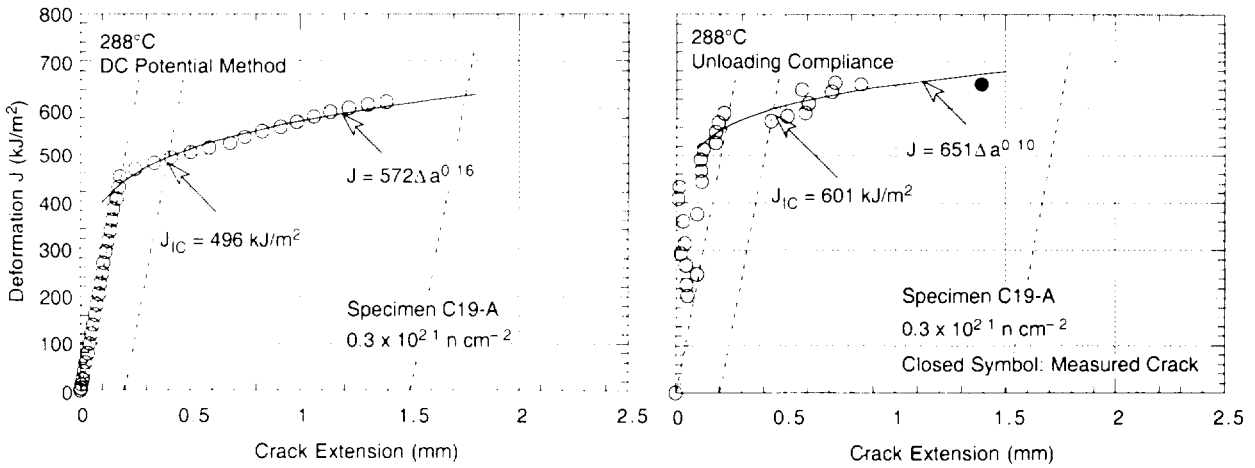
Figure 26. Fracture toughness J-R curves determined by DC-potential-drop and unloading compliance methods for Heat C19 of Type 304 SS irradiated to 0.3 x 10^{21} n·cm^{-2} at 288 C. Dashed lines represent the blunting line and 0.2- and 1.5-mm offset lines.
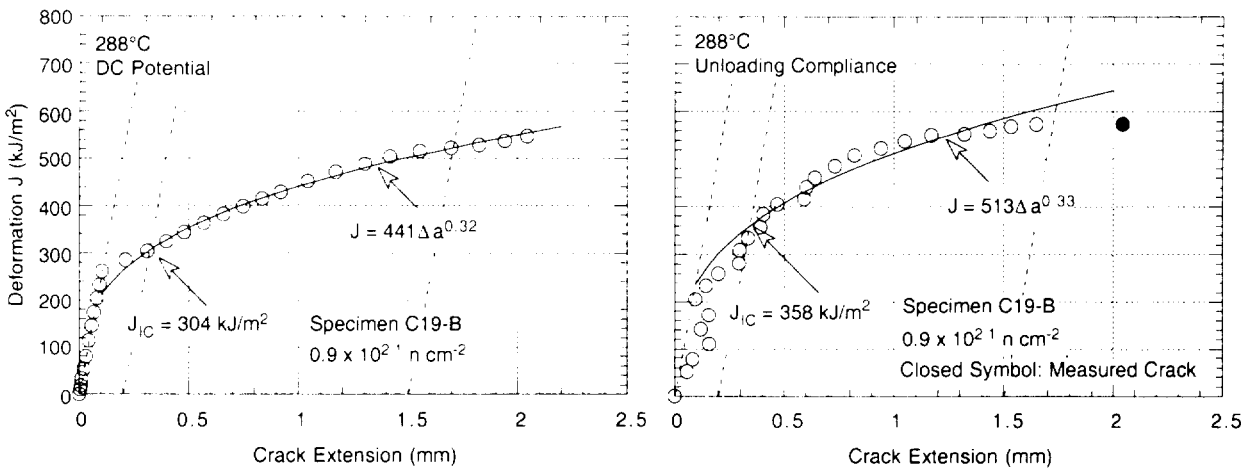
Figure 27. Fracture toughness J-R curves determined by DC-potential-drop and unloading compliance methods for Heat C19 of Type 304 SS irradiated to 0.9 x 10^{21} n·cm^{-2} at 288°C. Dashed lines represent the blunting line and 0.2- and 1.5-mm offset lines.
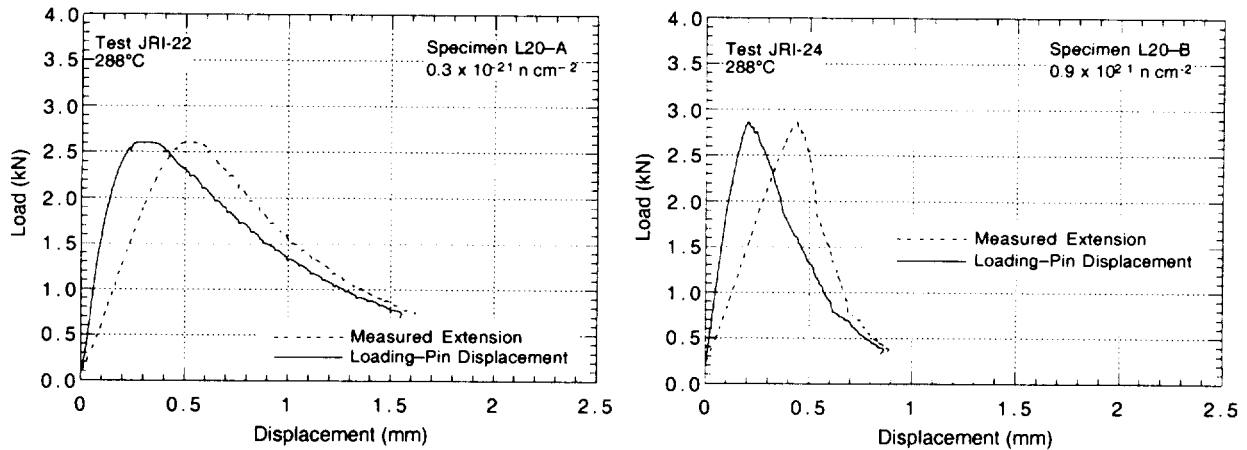
Figure 28. Load-vs.-loadline-displacement curves for Heat L20 of Type 304 SS irradiated to 0.3 and 0.9 x 10^{21} n·cm^{-2} in the Halden reactor at 288°C
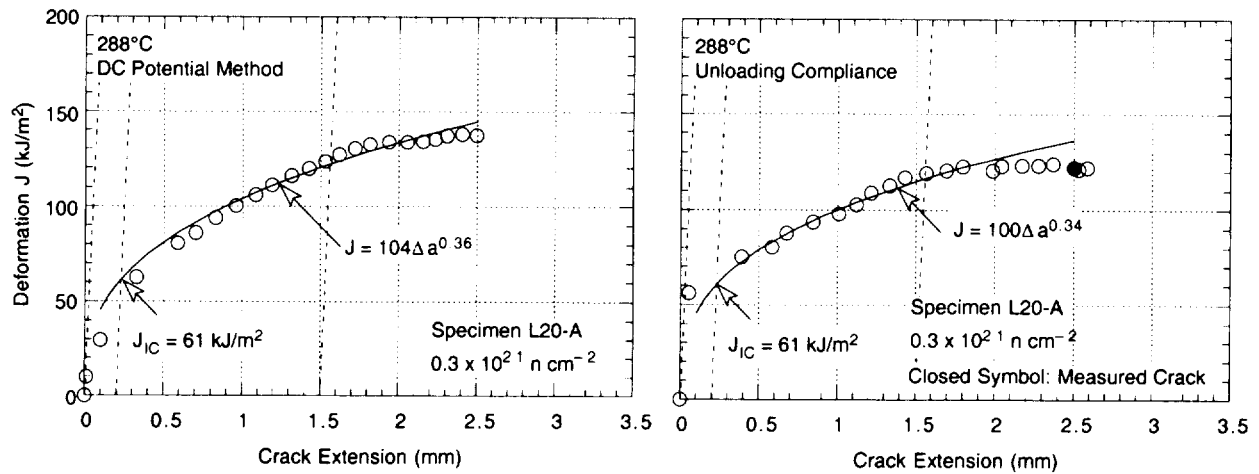
Figure 29. Fracture toughness J-R curves determined by DC-potential-drop and unloading compliance methods for Heat L20 of Type 304 SS irradiated to 0.3 x 10^{21} n·cm^{-2} at 288°C. Dashed lines represent the blunting line and 0.2- and 1.5-mm offset lines.
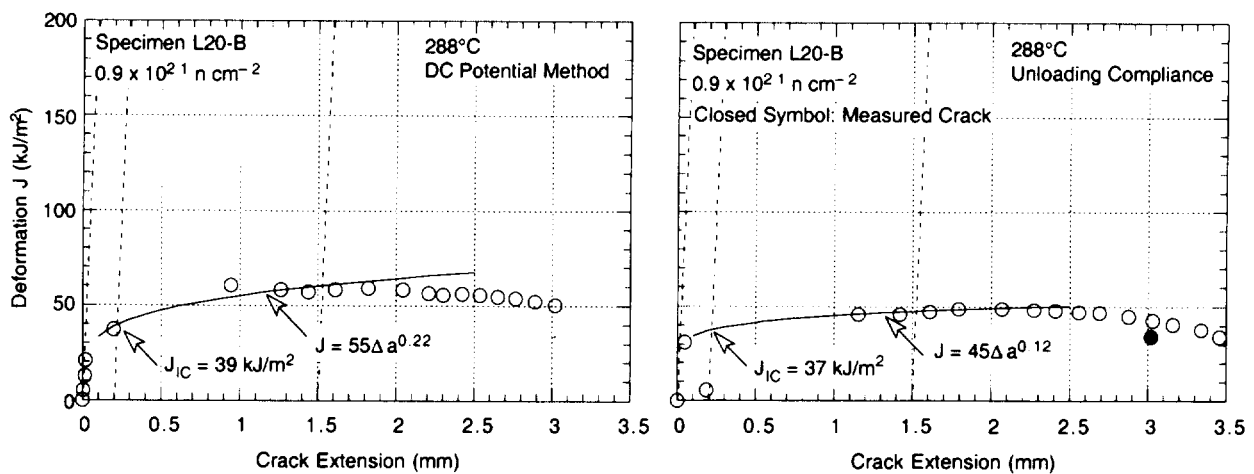
Figure 30. Fracture toughness J-R curves determined by DC-potential-drop and unloading compliance methods for Heat L20 of Type 304 SS irradiated to 0.9 x 10^{21} n·cm^{-2} at 288°C. Dashed lines represent the blunting line and 0.2- and 1.5-mm offset lines.

33
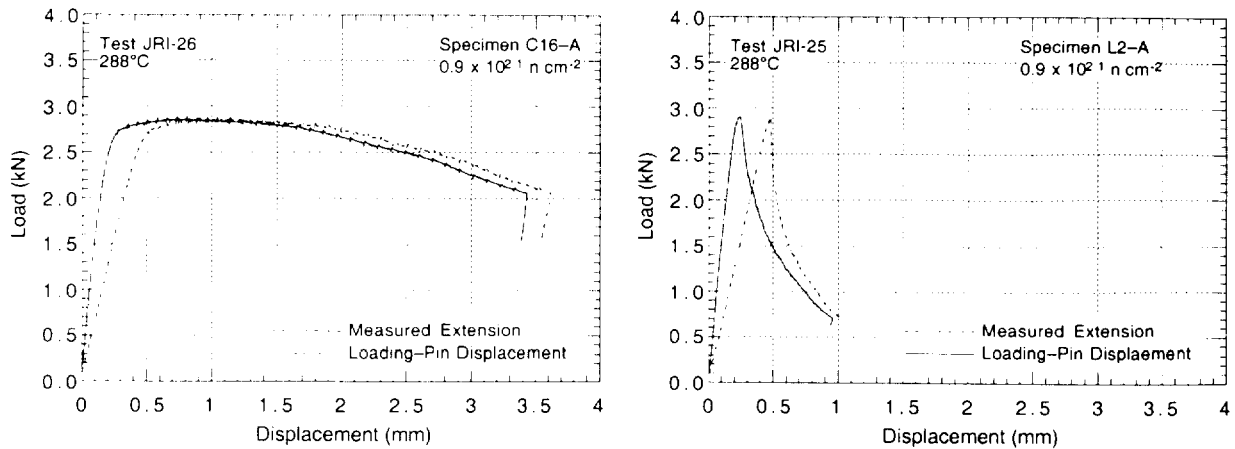
Figure 31. Load-vs.-loadline-displacement curves for Heats C16 and L2 of Type 304 SS irradiated to 0.9 x 10²¹ n·cm⁻² in the Halden reactor at 288°C
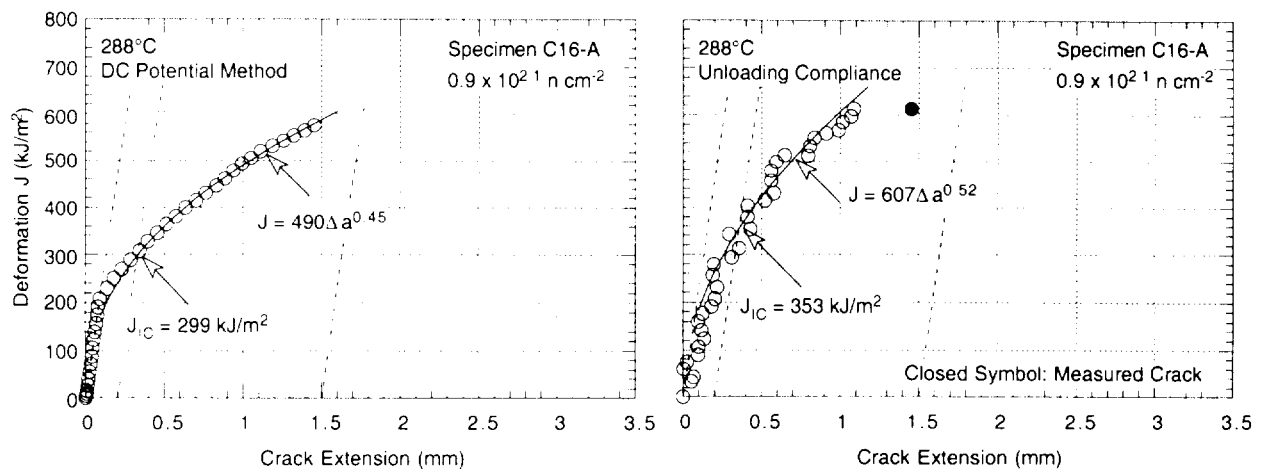
Figure 32. Fracture toughness J-R curves determined by DC-potential-drop and unloading compliance methods for Heat C16 of Type 304 SS irradiated to 0.9 x 10²¹ n·cm⁻² at 288°C. Dashed lines represent the blunting line and 0.2- and 1.5-mm offset lines.
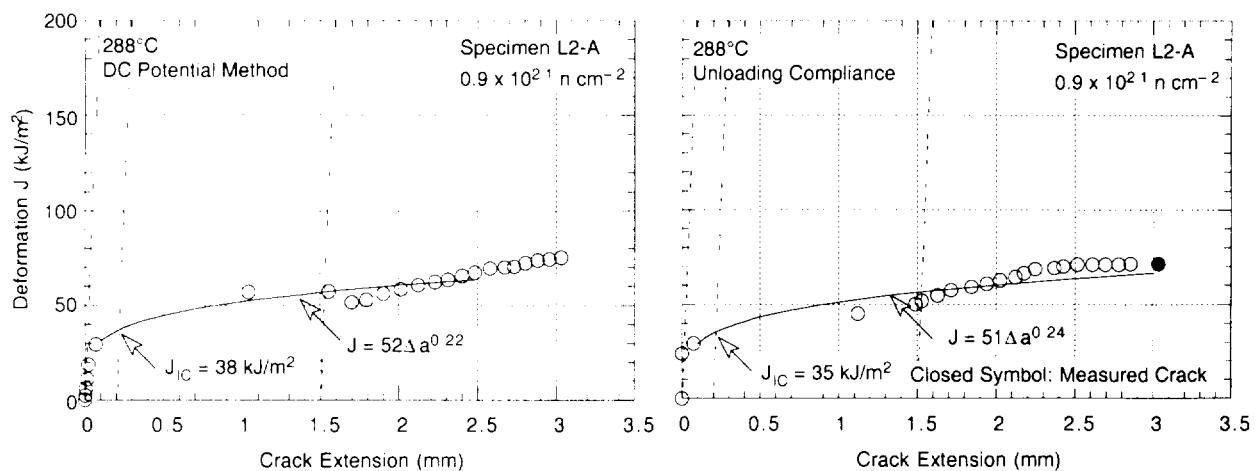
Figure 33. Fracture toughness J-R curves determined by DC-potential-drop and unloading compliance methods for Heat L2 of Type 304 SS irradiated to 0.9 x 10²¹ n·cm⁻² at 288°C. Dashed lines represent the blunting line and 0.2- and 1.5-mm offset lines.

condition, the differences between the fracture toughness of the irradiated commercial and laboratory heats most likely arise from differences in toughness of the nonirradiated steels.

The experimental J_{ic} values for the four heats are plotted as a function of neutron exposure in Fig. 34. The results for irradiated Type 304 SS reactor internal material from operating BWRs are also included in the figure. The fracture toughness results at 288°C are consistent with a saturation J_{ic} value of ≈ 30 kJ/m^2 (or K_{jc} of 70 MPa·m$^{0.5}$).
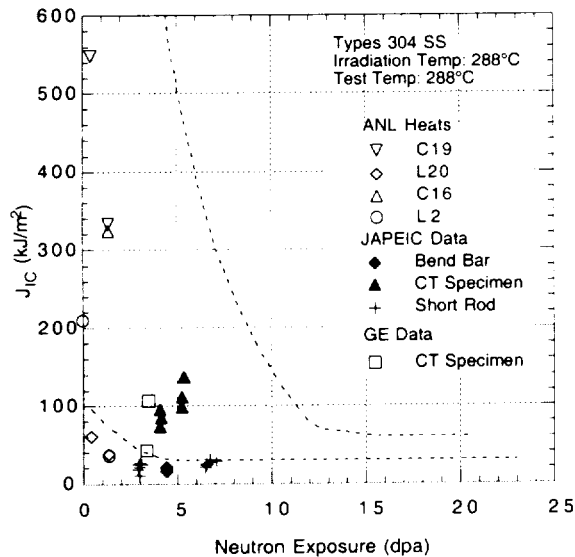
Figure 34.

Fracture toughness J_{IC} of austenitic stainless steels as a function of neutron exposure at 288°C. Dashed lines represent upper and lower bounds for change in J_{ic} for austenitic SSs irradiated at 350–450°C. JAPEIC = Japan Power Engineering and Inspection Corporation, GE = General Electric Nuclear Energy

3.4.3 Conclusions

Fracture toughness J–R curve tests have been conducted on four heats of Type 304 stainless steel that were irradiated to fluence levels of ≈ 0.3 and 0.9×10^{21} n·cm^{-2} (E > 1 MeV) at ≈ 288°C in a He environment in the Halden boiling–heavy–water reactor. The tests were performed on 1/4–T CT specimens in air at 288°C; crack extensions were determined by the DC–potential and elastic unloading compliance techniques. Neutron irradiation at 288°C to 0.9×10^{21} n·cm^{-2} decreased the fracture toughness of all of the steels. Minor differences in the chemical composition of the steels, e.g., differences in Ni content for Heats C16 and C19 or Si content for Heats L2 and L20, have little or no effect on the fracture toughness of irradiated steels. The Commercial Heats C16 and C19 exhibited fracture toughness that is superior to the fracture toughness of the Laboratory Heats L20 and L2. For steels irradiated to 0.9×10^{21} n·cm^{-2}, the J_{ic} values are 326 and 331 kJ/m^2, respectively, for Heats C16 and C19, and 36 and 38 kJ/m^2, respectively, for Heats L2 and L20.

4 Environmentally Assisted Cracking of Alloys 600 and 690 in Simulated LWR Water
(W. E. Ruther, W. K. Soppet, T. F. Kassner, and W. J. Shack)

The objective of this work is to evaluate the resistance of Alloys 600 and 690 to EAC in simulated LWR coolant environments. High–Ni alloys have experienced general corrosion (tube wall thinning), localized intergranular attack (IGA), and SCC in LWRs. Secondary–side IGA* and axial and circumferential SCC** have occurred in Alloy 600 tubes at tube support plates in many steam generators. Primary–water SCC of Alloy 600 steam generator tubes in PWRs at roll transitions and U–bends and in tube plugs*** is a widespread problem that has been studied intensively. Cracking has also occurred in Alloy 600 and other high–Ni alloys (e.g., Inconel–82 and –182 and Alloy X750) that are used in applications such as instrument nozzles and heater thermal sleeves in the pressurizer[†] and the penetrations for control–rod drive mechanisms in reactor vessel closure heads in the primary system of PWRs;[††] in dissimilar–metal welds between SS piping and LAS nozzles, in jet pump hold–down beams,[†††] and in shroud–support–access–hole covers[§] in BWRs. Alloy 600, in general, undergoes differing thermomechanical processing for applications other than steam generator tubes. Because environmental degradation of the alloys in many cases is very sensitive to processing, further evaluation of even SCC is needed. In addition, experience strongly suggests that materials that are susceptible to SCC are also susceptible to environmental degradation of fatigue life and fatigue–crack growth properties. During this investigation, we obtained information on the effect of temperature, load ratio R, and stress intensity (K) on EAC of Alloys 600 and 690 in simulated BWR and PWR water. Correlations for crack growth rates (CGRs) were developed; they were based on the best fit of the data to equations that incorporate relevant loading parameters and the DO level in water.

4.1 Crack Growth Rates of Alloys 600 and 690 in Air and Water

Crack growth experiments have been performed on Alloys 600 and 690 to explore the effects of temperature, stress ratio, stress intensity, and water chemistry on CGRs. These data have been summarized elsewhere.[88–91] Baseline CGR tests were performed in air at several

---

*USNRC Information Notice No. 91–67, "Problems with the Reliable Detection of Intergranular Attack (IGA) of Steam Generator Tubing," Oct. 1991.

**USNRC Information Notice No. 90–49, "Stress Corrosion Cracking in PWR Steam Generator Tubes," Aug. 1990: Notice No. 91–43, "Recent Incidents Involving Rapid Increases in Primary–to–Secondary Leak Rate," July 1991; Notice No. 92–80, "Operation with Steam Generator Tubes Seriously Degraded," Dec. 1992; Notice No. 94–05, "Potential Failure of Steam Generator Tubes with Kinetically Welded Sleeves," Jan. 1994.

***USNRC Information Notice No. 89–33, "Potential Failure of Westinghouse Steam Generator Tube Mechanical Plugs," March 1989; Notice No. 89–65, "Potential for Stress Corrosion Cracking in Steam Generator Tube Plugs Supplied by Babcock and Wilcox," Sept. 1989; Notice No. 94–87, "Unanticipated Crack in a Particular Heat of Alloy 600 Used for Westinghouse Mechanical Plugs for Steam Generator Tubes," Dec. 1994.

[†]USNRC Information Notice No. 90–10, "Primary Water Stress Corrosion Cracking (PWSCC) of Inconel 600," Feb. 1990.

[††]USNRC Generic Letter 97-01: "Degradation of Control Rod Drive Mechanism and Other Vessel Closure Head Penetrations," Apr. 1, 1997; USNRC Information Notice No. 96–11, "Ingress of Demineralizer Resins Increases Potential for Stress Corrosion Cracking of Control Rod Drive Mechanism Penetrations," Feb. 1996; INPO Document SER 20–93 "Intergranular Stress Corrosion Cracking of Control Rod Drive Mechanism Penetrations," Sept. 1993.

[†††]USNRC Information Notice 93–101, "Jet Pump Hold–Down Beam Failure," Dec. 1993.

[§]USNRC Information Notice 92–57, "Radial Cracking of Shroud Support Access Hole Cover Welds," Aug. 1992.

temperatures between 35 and 380°C. Correlations for the CGRs of Alloys 600 and 690 as a function of the range of stress intensity factor ΔK, stress ratio R, and DO level have also been developed.[89] Because these data were obtained only for a single rise time, alternate forms for the correlations were also chosen to extrapolate the results to other rise times, i.e., frequencies.[90] The CGRs of Alloys 600 and 690 in air can be expressed by the equation

$$CGR_{air} = \left(\frac{1}{t_r}\right)\frac{da}{dN} = \left(\frac{1}{t_r}\right)D(1 - bR)^P\Delta K^n,$$ (4)

where $R = K_{min}/K_{max}$, $\Delta K = K_{max}(1-R)$, t_r is the rise time of the loading waveform, and D, b, p, and n are empirical parameters. The values of these parameters for Alloys 600 and 690 are listed in Table 8.

Table 8. Constants in CGR equations in air ($T \leq 289°C$)

Alloy	D (m·s^{-1})	b	p	n
600	1.64 x 10^{-13}	0.82	-1.74	3.80
690	2.23 x 10^{-13}	0.83	-1.51	3.80
600 and 690	1.92 x 10^{-13}	0.83	-1.62	3.80

Ford and Andresen[92,93] argue that there are fundamental reasons to expect that the CGRs for these alloys in LWR environments should be of the form

$$CGR_{env} = CGR_{air} + A(\dot{\varepsilon}_T)^m,$$ (5)

where CGR_{env} is the CGR in the environment, CGR_{air} is the CGR in air (a relatively inert environment), and $\dot{\varepsilon}_T$ is the crack tip strain rate. The parameters A and m depend on the material and the environment. Shoji has argued that under cyclic loading, $\dot{\varepsilon}_T$ is proportional to CGR_{air}.[94] Thus, Eq. 5 can be written as

$$CGR_{env} = CGR_{air} + A(CGR_{air})^m,$$ (6)

which is a convenient form for comparisons with experimental data and which has been widely used to correlate CGR data.[95-97] The best-fit values of parameters A and m in Eq. 6 for Alloys 600 and 690 in various environments are summarized in Table 9.

Table 9. "Best fit" values for parameters A and m in Eq. 21 for Alloys 600 and 690

Alloy	Environment	A	m
600 Low C	High and low DO	1.5 x 10^{-5}	0.48
600	Low DO	2.1 x 10^{-8}	0.33
600	300 ppb DO	4.4 x 10^{-7}	0.33
600	300 ppb DO + impurities	1.9 x 10^{-6}	0.33
600	6 ppm DO	7.7 x 10^{-7}	0.33
690	Low DO	2.1 x 10^{-7}	0.33
690	6 ppm DO	4.4 x 10^{-7}	0.33

The CGRs in the low-C heat of Alloy 600 do not appear to be sensitive to either heat treatment or DO level, and the entire data set was fit with a single set of parameters. The three heats of Alloy 600, with ≈0.06 wt.% C, in either a solution-annealed or mill-annealed

condition, show strong environmental enhancement in high–DO environments. The situation is less clear in low–DO environments. Some tests under loading conditions that would produce CGRs in air of $\approx 10^{-11}$–10^{-10} m·s^{-1} show enhancement, others do not. Fewer tests of these materials have been performed in low–DO environments at the very low CGRs that might be expected to show a greater degree of environmental enhancement.

Alloy 690 in either the solution–annealed condition or after thermal treatment, shows only a modest enhancement in low–DO environments (which include both high–purity water and water with H_3BO_3 and LiOH additions); the enhancement appears to be independent of the loading conditions as long as $CGR_{air} \geq 10^{-11}$ s^{-1}. The CGRs in high–DO water seem to be consistent with the CGR_{air} model, although the data are sparse. Some environmental enhancement occurs under loading conditions that correspond to low CGRs in air.

The crack growth data for Alloy 600 and 690 specimens under constant load in high–DO water (i.e., ≈ 300 ppb DO) show little or no effect of the stress intensity factor K on growth rates at K values of 27–30 MPa·m$^{1/2}$, Fig. 35(a). For Alloy 600, the CGRs are influenced by thermal treatment; growth rates for the hot–worked Alloy 600 are a factor of ≈ 5 greater than those for the hot–worked + thermally treated Alloy 600. The addition of sulfate increased the CGRs of Alloy 600 in both heat treatment conditions by a factor of 3–7. The CGRs for Alloy 690 range between $\approx 2 \times 10^{-12}$ and 6×10^{-12} m/s; however, these values may be below the sensitivity of the crack–length monitoring system. Also, the addition of sulfates exerted no effect on the growth rates of Alloy 690.
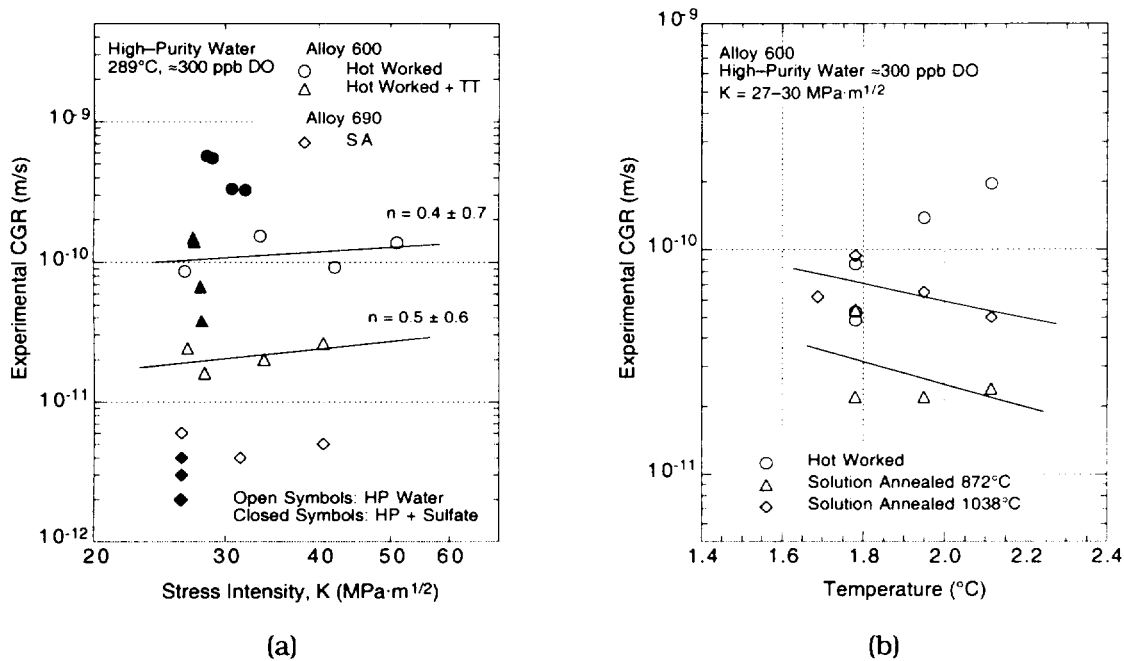
Figure 35. *Effect of (a) stress intensity factor K and (b) temperature on crack growth rates of Alloys 600 and 690 in high–purity water with ≈ 300 ppb DO at 289°C*

Between 200 and 320°C, the CGRs in solution–annealed Alloy 600 are weakly dependent on temperature, Fig. 35(b). Although there is considerable uncertainty because the data set is small and the data are scattered, these CGRs appear to increase slightly with increasing temperature. However, the growth rates in hot–worked Alloy 600 (20% reduction) decrease

significantly with temperature and become comparable to those in the solution–annealed materials. A decrease in the CGRs of SCC in simulated BWR environments at temperatures above 288°C has been observed in austenitic SSs.[98,99] In that case, however, the decrease was much greater and produced CGRs $<10^{-11}$ m/s in the SS.

4.2 Crack Growth Rates of Alloy 690 in High–DO Water

The experimental effort during the current reporting period was focused on fatigue CGRs of Alloy 690 in high–purity water at 289°C. The heat numbers, heat and heat-treatment identification code, product form, and source of materials for fabrication of 1–T CT specimens are presented in Table 10. The composition and tensile properties of the alloys are listed in Tables 11 and 12, respectively.

Table 10. Product form and source of Alloy 690

Alloy	Heat No.	Material Condition	Heat/Heat Treat. Code	Product Form	Source
690	NX8244HK-1B	Annealed 1093°C/1 h	11	1.0-in.-thick plate	EPRI[a]

[a]INCO Alloys Intl., Inc. of Huntington, WV, produced numerous heats of Alloys 600 and 690 for the Electric Power Research Institute (EPRI), Palo Alto, CA, which provided material for this study.

Table 11. Composition (wt.%) of Alloy 690 for corrosion fatigue tests

Heat	Cr	Mo	Ni	Fe	Mn	Si	C	N	P	S	Cu	Ti	Al	Co	Nb+Ta
NX8244HK 1B	30.64	<0.01	59.20	9.19	0.21	0.18	0.023	0.011	0.005	0.002	<0.01	0.19	0.32	<0.01	<0.01

Table 12. Tensile properties[a] of Alloy 690 at various temperatures

Heat No.	Material Condition	Temp. (°C)	σ_y (MPa)	σ_u (MPa)	ε_t (%)	RA (%)	Hardness (R_B)	ASTM Grain Size
NX8244HK-1B	Annealed 1093°C/1 h	25[b]	212.3	602.8	59.0	–	70	–
		25	215.6	592.2	70.5	71.6	78	2
		290	145.2	504.9	70.6	68.1	–	–
		320	150.9	499.4	67.1	67.3	–	–

[a]Tensile tests conducted in air at a strain rate of 1.0 x 10-4 s-1.
[b]Results from vendor documents.

A crack growth test has been conducted on Alloy 690 (Heat NX8244HK, solution annealed at 1093°C for 1 h) under cyclic loading in high–purity water with ≈350 ppm DO at 289°C, load ratio R = 0.7, ΔK ≈11.5, and rise times of 12, 60, 300, and 1000 s; the results are presented in Table 13. The CGRs measured in water and those predicted in air for the same loading conditions are plotted in Fig. 36. The data obtained earlier on Heat HX8662HG (mill annealed and heat treated at 715°C for 5 h) are also included in the figure. The CGRs in air were determined from Eq. 4. The results indicate that the CGRs of Alloy 690 in high–DO water are a factor of ≈4 greater than those in air independent of frequency.

Table 13. Crack growth results for Alloy 690[a] in high-purity at 289°C

Test No.	Test Time, h	O_2[b] Conc. ppb	Cond. at 25°C, μS/cm	pH at 25°C	Electrode Potential mV(SHE) at 289°C		Load Ratio	Rise Time s	K_{max}[c], Mpa·m$^{1/2}$	ΔK, Mpa·m$^{1/2}$	Growth Rate, 10^{-10} m/s
					304 SS	Pt					
1	645–745	320	≈0.07	–	–	–	0.4	12	26.0	15.6	16.70
2	747–797	325	≈0.07	–	–	–	0.4	12	22.2	13.3	0.50
3	797–847	298	≈0.07	–	–	–	0.2	12	23.2	18.6	1.92
4	847–985	312	≈0.07	–	–	–	0.2	12	23.5	18.8	5.93
5	985–1134	329	≈0.07	–	–	–	1.0	–	37.7	–	–
6	1134–1156	287	≈0.07	–	–	–	0.7	12	38.1	11.4	17.5
7	1160–1255	348	≈0.07	–	–	–	0.7	60	38.4	11.5	4.91
8	1255–1465	346	≈0.07	–	–	–	0.7	300	38.5	11.6	1.01
9	1466–1493	355	≈0.07	–	–	–	0.7	12	38.9	11.7	20.2
10	1493–1583	390	≈0.07	6.3	–	–	0.7	60	39.3	11.8	5.80
11	1583–1778	364	≈0.07	6.3	–	–	0.7	300	39.6	11.9	1.15
12	1778–2111	375	≈0.07	6.3	–	–	0.7	1000	39.7	11.9	0.41

[a]CT specimen of Alloy 690 Heat No. NX8244HK, solution annealed 1093°C for 1 h. Yield stress at 289°C = 145 MPa.
[b]Effluent DO concentration was determined with an Orbisphere DO monitor.
[c]Stress intensity, Kmax, values at the end of the time period.
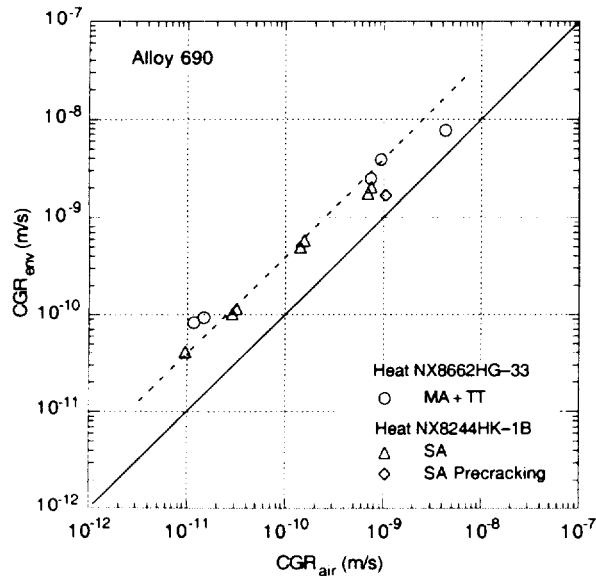
Figure 36.
Predicted and measured CGRs for Alloy 690 in high-purity water at 289°C

5 Summary of Results

5.1 Environmental Effects on Fatigue S–N Behavior of Primary Pressure Boundary Materials

Fatigue tests have been conducted on Type 304 SS in high–purity water at 288°C to study the effects of water chemistry on the fatigue life of these steels. The results indicate that for wrought austenitic SSs, environmental effects on fatigue life are more pronounced in low–DO, i.e., <0.01 ppm DO, than in high–DO, i.e., ≥0.1 ppm DO, water. In high–DO water, environmental effects are moderate (less than a factor of 2 decrease in life) when conductivity is maintained at <0.1 μS/cm and ECP of the steel has reached a stable value. For fatigue tests in high–DO water, the SS specimens must be soaked for ≈5 days for the ECP of the steel to reach a stable value. In low–DO water, the addition of Li and B, or low conductivity, or preexposing the specimen for ≈5 days before the test, or dissolved H, have no effect on fatigue life of austenitic SSs. Additional fatigue tests are being conducted in high–DO water at 288°C to confirm these results.

5.2 Irradiation–Assisted Stress Corrosion Cracking of Austenitic Stainless Steels

Slow-strain-rate tensile tests in simulated BWR water (DO ≈8 ppm) were conducted on model austenitic SS alloys that were irradiated at 289°C in He in the Halden boiling-heavy-water reactor to a fluence of ≈0.9 x 10^{21} n·cm^{-2} (E > 1 MeV). Fractographic analysis by SEM was conducted to determine the susceptibility to IASCC, as manifested by the degree of IG fracture surface morphology. Heat-to-heat variations in ductility and susceptibility of the irradiated steels to IGSCC were very significant. This finding indicates that heat-to-heat variation in CGR could also be strong. A Type 304 SS alloy that contains a high concentration of O exhibited high susceptibility to IASCC. A few Type 304 SS alloys that contain high concentrations of Si in the range of 1.1 to 1.5 wt.%, exhibited negligible susceptibility to IGSCC. The beneficial effect of high concentrations of Cr was very significant, that is, alloys that contain <15.5 wt.% Cr exhibited relatively higher susceptibility to IASCC, whereas an alloy that contains >21 wt.% Cr exhibited relatively lower susceptibility than other alloys.

Certain safety-related core internal structural components accumulate very high levels of irradiation damage (20-100 displacement per atom or dpa) by the end of life. Data bases and our mechanistic understanding of the degradation of such highly irradiated components, however, are not well established. A key question is the nature of irradiation-assisted IG cracking at very high dose, i.e., is it purely mechanical failure or SCC. To provide a better understanding of IASCC at very high fluence, hot-cell tests and microstructural characterization were performed on Type 304 SS specimens obtained from the hexagonal fuel can of the decommissioned EBR-II reactor after irradiation to ≈50 dpa at ≈370°C. Slow-strain-rate tensile tests were conducted at 289°C in air and in water at several levels of ECP, and microstructural characteristics were analyzed by SEM and TEM. The 50-dpa-irradiated steel deformed significantly by twinning and exhibited surprisingly high ductility in air, but was susceptible to severe IGSCC at high ECP. Low levels of DO and ECP were effective in suppressing the susceptibility of the heavily irradiated material to IGSCC, indicating that the stress corrosion process associated with irradiation-induced grain-boundary Cr depletion, rather than purely mechanical separation of grain boundaries, plays the dominant role. However, although IGSCC was suppressed, the material was susceptible to dislocation

channeling at low ECP, and this susceptibility led to poor work-hardening capability and low ductility.

Fracture toughness J–R curve tests have been conducted on two commercial and two laboratory heats of Type 304 SS that were irradiated to fluence levels of ≈ 0.3 and 0.9×10^{21} n·cm^{-2} (E > 1 MeV) at $\approx 288°C$ in a He environment in the Halden boiling–heavy–water reactor. The tests were performed on 1/4–T CT specimens in air at 288°C, crack extensions were determined by both DC–potential–drop and elastic unloading compliance techniques. Neutron irradiation at 288°C to 0.9×10^{21} n·cm^{-2} decreased the fracture toughness of all of the steels. Minor differences in the chemical composition of the steels, e.g., differences in Ni or Si content, have little or no effect on the fracture toughness of irradiated steels. The commercial heats exhibited fracture toughness that is superior to the fracture toughness of the laboratory heats. For steels irradiated to 0.9×10^{21} n·cm^{-2}, the Jic values are 326 and 331 kJ/m2, respectively, for the two commercial heats, and 36 and 38 kJ/m^2, respectively, for the two laboratory heats.

5.3 Environmentally Assisted Cracking of Low–Carbon Alloys 600 and 690 in Simulated LWR Water

To evaluate the resistance of Alloys 600 and 690 to EAC in LWR coolant environments, fracture mechanics CGR tests are being conducted in air and water environments on CT specimens of several heats of these alloys in annealed and in annealed and thermally treated conditions. A statistical analysis of the results was used to develop correlations for predicting CGRs of the materials as a function of stress intensity, stress ratio, and DO levels. However, because the experimental data were obtained for only a single rise time, i.e., frequency, alternate forms for the correlations have also been developed to extrapolate the results to other rise times.

The CGRs in the low–C heat of Alloy 600 do not appear to be sensitive to either heat treatment or DO level, whereas the CGRs in the high–C heats show a strong environmental enhancement in high–DO environments. The results are inconclusive for the high–C Alloy 600 in low–DO environments. Alloy 690 shows only a modest environmental enhancement in low–DO environments; environmental effects appear to be independent of the loading conditions as long as $CGR_{air} \geq 10^{-11}$ m/s. The CGRs in Alloy 690 in high–DO show some environmental enhancement for loading conditions that correspond to low CGRs in air.

The crack growth data for Alloy 600 and 690 specimens under constant load in high–DO water (i.e., ≈ 300 ppb DO) show little or no effect of the stress intensity factor K on growth rates at K values of 27–30 MPa·m$^{1/2}$. For Alloy 600, the CGRs are influenced by thermal treatment; growth rates for the hot–worked Alloy 600 are a factor of ≈ 5 greater than those for the hot–worked + thermally treated Alloy 600. The addition of sulfate increased the CGRs of Alloy 600 under both heat treatment conditions by a factor of 3–7. The CGRs for Alloy 690 range between $\approx 2 \times 10^{-12}$ and 6×10^{-12} m/s; however, these values may be below the sensitivity of the crack length monitoring system. Also, the addition of sulfates exerted no effect on the CGRs of Alloy 690.

The experimental effort during the current reporting period was focused on the effects of rise time on fatigue CGRs of Alloy 690 in high–purity water at 289°C. A crack growth test has been conducted on a CT specimen of Alloy 690 under cyclic loading in high–purity water with

≈350 ppm DO at 289°C, load ratio R = 0.7, $\Delta K \approx 11.5$ MPa·m$^{1/2}$, and rise times of 12, 60, 300, and 1000 s. The results indicate that the CGRs of Alloy 690 in high–DO water are a factor of ≈4 greater than those in air.

References

1. K. Iida, *A Review of Fatigue Failures in LWR Plants in Japan*, Nucl. Eng. Des. **138**, 297–312 (1992).

2. K. Kussmaul, R. Rintamaa, J. Jansky, M. Kemppainen, and K. Törrönen, *On the Mechanism of Environmental Cracking Introduced by Cyclic Thermal Loading*, in IAEA Specialists Meeting Corrosion and Stress Corrosion of Steel Pressure Boundary Components and Steam Turbines, VTT Symp. 43, Espoo, Finland, pp. 195–243 (1983).

3. K. Kussmaul, D. Blind, and J. Jansky, *Formation and Growth of Cracking in Feed Water Pipes and RPV Nozzles*, Nucl. Eng. Des. **81**, 105–119 (1984).

4. E. Lenz, B. Stellwag, and N. Wieling, *The Influence of Strain-Induced Corrosion Cracking on the Crack Initiation in Low Alloy Steels in HT-Water – A Relation Between Monotonic and Cyclic Crack Initiation Behavior*, in IAEA Specialists Meeting Corrosion and Stress Corrosion of Steel Pressure Boundary Components and Steam Turbines, VTT Symp. 43, Espoo, Finland, pp. 243–267 (1983).

5. *ASME Boiler and Pressure Vessel Code Section III – Rules for Construction of Nuclear Power Plant Components*, The American Society of Mechanical Engineers, New York, 1992 Ed.

6. B. F. Langer, *Design of Pressure Vessels for Low-Cycle Fatigue*, ASME J. Basic Eng. **84**, 389–402 (1962).

7. *Tentative Structural Design Basis for Reactor Pressure Vessels and Directly Associated Components (Pressurized, Water Cooled Systems)*, PB 151987, U.S. Dept. of Commerce, Office of Technical Service, 1 Dec. 1958 Revision.

8. S. Ranganath, J. N. Kass, and J. D. Heald, *Fatigue Behavior of Carbon steel Components in High-Temperature Water Environments*, in BWR Environmental Cracking Margins for Carbon Steel Piping, EPRI NP-2406, Electric Power Research Institute, Palo Alto, CA, Appendix 3 (May 1982).

9. W. A. Van Der Sluys, *Evaluation of the Available Data on the Effect of the Environment on the Low-Cycle Fatigue Properties in Light Water Reactor Environments*, in Proc. 6th Intl. Symp. on Environmental Degradation of Materials in Nuclear Power Systems – Water Reactors, R. E. Gold and E. P. Simonen, eds., The Metallurgical Society, Warrendale, PA, pp. 1–4 (1993).

10. N. Nagata, S. Sato, and Y. Katada, *Low-Cycle Fatigue Behavior of Pressure Vessel Steels in High-Temperature Pressurized Water*, ISIJ Intl. **31** (1), 106–114 (1991).

11. M. Higuchi and K. Iida, *Fatigue Strength Correction Factors for Carbon and Low-Alloy Steels in Oxygen-Containing High-Temperature Water*, Nucl. Eng. Des. **129**, 293–306 (1991).

12. M. Higuchi, K. Iida, and Y. Asada, *Effects of Strain Rate Change on Fatigue Life of Carbon Steel in High–Temperature Water*, in Fatigue and Crack Growth: Environmental Effects, Modeling Studies, and Design Considerations, PVP Vol. 306, S. Yukawa, ed., American Society of Mechanical Engineers, New York, pp. 111–116 (1995); also in Proc. Symp. on Effects of the Environment on the Initiation of Crack Growth, ASTM STP 1298, American Society for Testing and Materials, Philadelphia (1997).

13. H. Kanasaki, M. Hayashi, K. Iida, and Y. Asada, *Effects of Temperature Change on Fatigue Life of Carbon Steel in High–Temperature Water*, in Fatigue and Crack Growth: Environmental Effects, Modeling Studies, and Design Considerations, PVP Vol. 306, S. Yukawa, ed., American Society of Mechanical Engineers, New York, pp. 117–122 (1995).

14. G. Nakao, H. Kanasaki, M. Higuchi, K. Iida, and Y. Asada, *Effects of Temperature and Dissolved Oxygen Content on Fatigue Life of Carbon and Low–Alloy Steels in LWR Water Environmen*, in Fatigue and Crack Growth: Environmental Effects, Modeling Studies, and Design Considerations, PVP Vol. 306, S. Yukawa, ed., American Society of Mechanical Engineers, New York, pp. 123–128 (1995).

15. O. K. Chopra and W. J. Shack, *Effects of LWR Environments on Fatigue Life of Carbon and Low–Alloy Steels*, in Fatigue and Crack Growth: Environmental Effects, Modeling Studies, and Design Considerations, PVP Vol. 306, S. Yukawa, ed., American Society of Mechanical Engineers, New York, pp. 95–109 (1995).

16. O. K. Chopra and W. J. Shack, *Evaluation of Effects of LWR Coolant Environments on Fatigue Life of Carbon and Low–Alloy Steels*, in Effects of the Environment on the Initiation of Crack Growth, ASTM STP 1298, W. A. Van Der Sluys, R. S. Piascik, and R. Zawierucha, eds., American Society for Testing and Materials, Philadelphia, pp. 247–266 (1997).

17. O. K. Chopra and W. J. Shack, *Low–Cycle Fatigue of Piping and Pressure Vessel Steels in LWR Environments*, Nucl. Eng. Des. **184**, 49–76 (1998).

18. O. K. Chopra and W. J. Shack, *Effects of LWR Coolant Environments on Fatigue Design Curves of Carbon and Low–Alloy Steels*, NUREG/CR–6583, ANL–97/18 (March 1998).

19. O. K. Chopra and W. J. Shack, *Fatigue Crack Initiation in Carbon and Low–Alloy Steels in Light Water Reactor Environments – Mechanism and Prediction*, in Fatigue, Environmental Factors, and New Materials, PVP Vol. 374, H. S. Mehta, R. W. Swindeman, J. A. Todd, S. Yukawa, M. Zako, W. H. Bamford, M. Higuchi, E. Jones, H. Nickel, and S. Rahman, eds., American Society of Mechanical Engineers, New York, pp. 155–168 (1998).

20. O. K. Chopra and W. J. Shack, *Overview of Fatigue Crack Initiation in Carbon and Low–Alloy Steels in Light Water Reactor Environments*, J. Pressure Vessel Technol. **121**, 49–60 (1999).

21. M. Fujiwara, T. Endo, and H. Kanasaki, *Strain Rate Effects on the Low–Cycle Fatigue Strength of 304 Stainless Steel in High–Temperature Water Environment; Fatigue Life: Analysis and Prediction*, in Proc. Intl. Conf. and Exposition on Fatigue, Corrosion Cracking, Fracture Mechanics, and Failure Analysis, ASM, Metals Park, OH, pp. 309–313 (1986).

22. H. Mimaki, H. Kanasaki, I. Suzuki, M. Koyama, M. Akiyama, T. Okubo, and Y. Mishima, *Material Aging Research Program for PWR Plants*, in Aging Management Through Maintenance Management, PVP Vol. 332, I. T. Kisisel, ed., American Society of Mechanical Engineers, New York, pp. 97–105 (1996).

23. H. Kanasaki, R. Umehara, H. Mizuta, and T. Suyama, *Fatigue Lives of Stainless Steels in PWR Primary Water*, Trans. 14th Intl. Conf. on Structural Mechanics in Reactor Technology (SMiRT 14), Lyon, France, pp. 473–483 (1997).

24. H. Kanasaki, R. Umehara, H. Mizuta, and T. Suyama, *Effects of Strain Rate and Temperature Change on the Fatigue Life of Stainless Steel in PWR Primary Water*, Trans. 14th Intl. Conf. on Structural Mechanics in Reactor Technology (SMiRT 14), Lyon, France, pp. 485–493 (1997).

25. M. Higuchi and K. Iida, *Reduction in Low–Cycle Fatigue Life of Austenitic Stainless Steels in High–Temperature Water*, in Pressure Vessel and Piping Codes and Standards, PVP Vol. 353, D. P. Jones, B. R. Newton, W. J. O'Donnell, R. Vecchio, G. A. Antaki, D. Bhavani, N. G. Cofie, and G. L. Hollinger, eds., American Society of Mechanical Engineers, New York, pp. 79–86 (1997).

26. M. Hayashi, *Thermal Fatigue Strength of Type 304 Stainless Steel in Simulated BWR Environment*, Nucl. Eng. Des. **184**, 135–144 (1998).

27. M. Hayashi, K. Enomoto, T. Saito, and T. Miyagawa, *Development of Thermal Fatigue Testing with BWR Water Environment and Thermal Fatigue Strength of Austenitic Stainless Steels*, Nucl. Eng. Des. **184**, 113–122 (1998).

28. O. K. Chopra and D. J. Gavenda, *Effects of LWR Coolant Environments on Fatigue Lives of Austenitic Stainless Steels*, in Pressure Vessel and Piping Codes and Standards, PVP Vol. 353, D. P. Jones, B. R. Newton, W. J. O'Donnell, R. Vecchio, G. A. Antaki, D. Bhavani, N. G. Cofie, and G. L. Hollinger, eds., American Society of Mechanical Engineers, New York, pp. 87–97 (1997).

29. O. K. Chopra and D. J. Gavenda, *Effects of LWR Coolant Environments on Fatigue Lives of Austenitic Stainless Steels*, J. Pressure Vessel Technol. **120**, 116–121 (1998).

30. O. K. Chopra and J. L. Smith, *Estimation of Fatigue Strain-Life Curves for Austenitic Stainless Steels in Light Water Reactor Environments*, in Fatigue, Environmental Factors, and New Materials, PVP Vol. 374, H. S. Mehta, R. W. Swindeman, J. A. Todd, S. Yukawa, M. Zako, W. H. Bamford, M. Higuchi, E. Jones, H. Nickel, and S. Rahman, eds., American Society of Mechanical Engineers, New York, pp. 249–259 (1998).

31. O. K. Chopra, *Effects of LWR Coolant Environments on Fatigue Design Curves of Austenitic Stainless Steels*, NUREG/CR-5704, ANL-98/31 (April 1999).

32. V. Pasupathi and R. W. Klingensmith, *Investigation of Stainless Steel Clad Fuel Rod Failures and Fuel Performance in the Connecticut Yankee Reactor*, EPRI NP-2119, Electric Power Research Institute, Palo Alto, CA (1981).

33. F. Garzarolli, D. Alter, P. Dewes, and J. L. Nelson, *Deformability of Austenitic Stainless Steels and Ni-Base Alloys in the Core of a Boiling and Pressurized Water Reactor*, in Proc. 3rd Int. Symp. on Environmental Degradation of Materials in Nuclear Power Systems - Water Reactors, R. E. Gold and E. P. Simonen, eds., The Minerals, Metals, and Materials Society, Warrendale, PA, pp. 657-664 (1993).

34. A. J. Jacobs, G. P. Wozadlo, K. Nakata, T. Yoshida, and I. Masaoka, *Radiation Effects on the Stress Corrosion and Other Selected Properties of Type-304 and Type-316 Stainless Steels*, in Proc. 3rd Int. Symp. on Environmental Degradation of Materials in Nuclear Power Systems - Water Reactors, G. J. Theus and J. R. Weeks, eds., The Metallurgical Society, Warrendale, PA, pp. 673-680 (1988).

35. M. P. Manahan, R. Kohli, J. Santucci, and P. Sipushi, *A Phenomenological Investigation of In-Reactor Cracking of Type 304 Stainless Steel Control Rod Cladding*, Nucl. Eng. Des. **113**, 297-321 (1989).

36. R. Katsura, M. Kodama, and S. Nishimura, *DL-EPR Study of Neutron Irradiation in Type 304 Stainless Steel*, Corrosion **48**, 384-390 (1992).

37. S. M. Bruemmer, L. A. Charlot, and E. P. Simpson, *Irradiation-Induced Chromium Depletion and Its Influence on Intergranular Stress Corrosion Cracking of Stainless Steels*, in Proc. 5th Int. Symp. on Environmental Degradation of Materials in Nuclear Power Systems - Water Reactors, D. Cubicciotti, E. P. Simonen, and R. Gold, eds., American Nuclear Society, La Grange Park, IL, pp. 821-826 (1992).

38. A. J. Jacobs, G. E. C. Bell, C. M. Shepherd, and G. P. Wozadlo, *High-Temperature Solution Annealing as an IASCC Mitigating Technique*, in Proc. 5th Int. Symp. on Environmental Degradation of Materials in Nuclear Power Systems - Water Reactors, D. Cubicciotti, E. P. Simonen, and R. Gold, eds., American Nuclear Society, La Grange Park, IL, pp. 917-934 (1992).

39. M. E. Indig, J. L. Nelson, and G. P. Wozadlo, *Investigation of Protection Potential against IASCC*, in Proc. 5th Int. Symp. on Environmental Degradation of Materials in Nuclear Power Systems - Water Reactors, D. Cubicciotti, E. P. Simonen, and R. Gold, eds., American Nuclear Society, La Grange Park, IL, p. 941-947 (1992).

40. M. Kodama, S. Nishimura, J. Morisawa, S. Shima, S. Suzuki, and M. Yamamoto, *Effects of Fluence and Dissolved Oxygen on IASCC in Austenitic Stainless Steels*, in Proc. 5th Int. Symp. on Environmental Degradation of Materials in Nuclear Power Systems - Water Reactors, D. Cubicciotti, E. P. Simonen, and R. Gold, eds., American Nuclear Society, La Grange Park, IL, p. 948-954 (1992).

41. H. M. Chung, W. E. Ruther, J. E. Sanecki, A. G. Hins, and T. F. Kassner, *Stress Corrosion Cracking Susceptibility of Irradiated Type 304 Stainless Steels*, in Effects of Radiation on Materials: 16th Int. Symp., ASTM STP 1175, A. S. Kumar, D. S. Gelles, R. K. Nanstad, and T. A. Little, eds., American Society for Testing and Materials, Philadelphia, pp. 851-869 (1993).

42. M. Kodama, K. Fukuya, and H. Kayano, *The Relationship of Grain Boundary Composition in Irradiated Type 304 SS to Neutron Fluence and IASCC*, in Effects of Radiation on Materials: 16th Int. Symp., ASTM STP 1175, A. S. Kumar, D. S. Gelles, R. K. Nanstad, and T. A. Little, eds., American Society for Testing and Materials, Philadelphia, pp. 889-901 (1993).

43. A. J. Jacobs, *Influence of Impurities and Alloying Elements on IASCC in Neutron Irradiated Austenitic Stainless Steels*, in Effects of Radiation on Materials: 16th Int. Symp., ASTM STP 1175, A. S. Kumar, D. S. Gelles, R. K. Nanstad, and T. A. Little, eds., American Society for Testing and Materials, Philadelphia, pp. 902-918 (1993).

44. R. D. Carter, D. L. Damcott, M. Atzmon, G. S. Was, S. M. Bruemmer, and E. A. Kenik, *Capabilities and Limitations of Analytical Methods Used to Measure Radiation-Induced Grain Boundary Segregation*, in Proc. 6th Int. Symp. on Environmental Degradation of Materials in Nuclear Power Systems - Water Reactors, R. E. Gold and E. P. Simonen, eds., The Minerals, Metals, and Materials Society, Warrendale, PA, pp. 501-509 (1993).

45. H. M. Chung, W. E. Ruther, J. E. Sanecki, and T. F. Kassner, *Grain-Boundary Microchemistry and Intergranular Cracking of Irradiated Austenitic Stainless Steels*, in Proc. 6th Int. Symp. on Environmental Degradation of Materials in Nuclear Power Systems - Water Reactors, R. E. Gold and E. P. Simonen, eds., The Minerals, Metals, and Materials Society, Warrendale, PA, pp. 511-519 (1993).

46. S. M. Bruemmer, J. I. Cole, J. L. Brimhall, R. D. Carter, and G. S. Was, *Radiation Hardening Effects on Localized Deformation and Stress Corrosion Cracking of Stainless Steels*, in Proc. 6th Int. Symp. on Environmental Degradation of Materials in Nuclear Power Systems - Water Reactors, R. E. Gold and E. P. Simonen, eds., The Minerals, Metals, and Materials Society, Warrendale, PA, pp. 537-545 (1993).

47. K. Fukuya, S. Shima, K. Nakata, S. Kasahara, A. J. Jacobs, G. P. Wozadlo, S. Suzuki, and M. Kitamura, *Mechanical Properties and IASCC Susceptibility in Irradiated Stainless Steels*, in Proc. 6th Int. Symp. on Environmental Degradation of Materials in Nuclear Power Systems - Water Reactors, R. E. Gold and E. P. Simonen, eds., The Minerals, Metals, and Materials Society, Warrendale, PA, pp. 564-572 (1993).

48. J. L. Cookson, D. L. Damcott, G. W. Was, and P. L. Andresen, *The Role of Microchemical and Microstructural Effects in the IASCC of High-Purity Austenitic Stainless Steels*, in Proc. 6th Int. Symp. on Environmental Degradation of Materials in Nuclear Power Systems - Water Reactors, R. E. Gold and E. P. Simonen, eds., The Minerals, Metals, and Materials Society, Warrendale, PA, pp. 573-580 (1993).

49. K. Kodama, R. Katsura, J. Morisawa, S. Nishimura, S. Suzuki, K. Asano, K. Fukuya, and K. Nakata, *IASCC Susceptibility of Austenitic Stainless Steels Irradiated to High Neutron Fluence*, in Proc. 6th Int. Symp. on Environmental Degradation of Materials in Nuclear Power Systems - Water Reactors, R. E. Gold and E. P. Simonen, eds., The Minerals, Metals, and Materials Society, Warrendale, PA, pp. 583-588 (1993).

50. A. J. Jacobs, G. P. Wozadlo, K. Nakata, S. Kasahara, T. Okada, S. Kawano, and S. Suzuki, *The Correlation of Grain Boundary Composition in Irradiated Stainless Steel with IASCC Resistance*, in Proc. 6th Int. Symp. on Environmental Degradation of Materials in Nuclear Power Systems - Water Reactors, R. E. Gold and E. P. Simonen, eds., The Minerals, Metals, and Materials Society, Warrendale, PA, pp. 597-606 (1993).

51. F. Garzarolli, P. Dewes, R. Hahn, and J. L. Nelson, *Deformability of High-Purity Stainless Steels and Ni-Base Alloys in the Core of a PWR*, in Proc. 6th Int. Symp. on Environmental Degradation of Materials in Nuclear Power Systems - Water Reactors, R. E. Gold and E. P. Simonen, eds., The Minerals, Metals, and Materials Society, Warrendale, PA, pp. 607-613 (1993).

52. S. Kasahara, K. Nakata, K. Fukuya, S. Shima, A. J. Jacobs, G. P. Wozadlo, and S. Suzuki, *The Effects of Minor Elements on IASCC Susceptibility in Austenitic Stainless Steels Irradiated with Neutrons*, in Proc. 6th Int. Symp. on Environmental Degradation of Materials in Nuclear Power Systems - Water Reactors, R. E. Gold and E. P. Simonen, eds., The Minerals, Metals, and Materials Society, Warrendale, PA, pp. 615-623 (1993).

53. M. Kodama, J. Morisawa, S. Nishimura, K. Asano, S. Shima, and K. Nakata, *Stress Corrosion Cracking and Intergranular Corrosion of Austenitic Stainless Steels Irradiated at 323 K*, J. Nucl. Mater., **1509**, 212-215 (1994).

54. T. Tsukada and Y. Miwa, *Stress Corrosion Cracking of Neutron Irradiated Stainless Steels*, in Proc. 7th Int. Symp. on Environmental Degradation of Materials in Nuclear Power Systems - Water Reactors, NACE International, Houston, pp. 1009-1018 (1995).

55. A. Jenssen and L. G. Ljungberg, *Irradiation–Assisted Stress Corrosion Cracking - Postirradiation CERT Tests of Stainless Steels in a BWR Test Loop*, in Proc. 7th Int. Symp. on Environmental Degradation of Materials in Nuclear Power Systems - Water Reactors, NACE International, Houston, 1043-1052 (1995).

56. F. Garzarolli, P. Dewes, R. Hahn, and J. L. Nelson, *In-Reactor Testing of IASCC Resistant Stainless Steels*, in Proc. 7th Int. Symp. on Environmental Degradation of Materials in Nuclear Power Systems - Water Reactors, NACE International, Houston, 1055-1065 (1995).

57. H. M. Chung, W. E. Ruther, J. E. Sanecki, A. G. Hins, and T. F. Kassner, *Effects of Water Chemistry on Intergranular Cracking of Irradiated Austenitic Stainless Steels*, in Proc. 7th Int. Symp. on Environmental Degradation of Materials in Nuclear Power Systems - Water Reactors, NACE International, Houston, p. 1133-1143 (1995).

58. K. Hide, T. Onchi, M. Mayazumi, K. Dohi, and Y. Futamura, *Intergranular Cracking of Irradiated Thermally Sensitized Type 304 Stainless Steel in High-Temperature Water and Inert Gas*, Corrosion **51**, 757-766 (1995).

59. H. M. Chung, W. E. Ruther, J. E. Sanecki, A. G. Hins, N. J. Zaluzec, and T. F. Kassner, *Irradiation–Assisted Stress Corrosion Cracking of Austenitic Stainless Steels: Recent Progress and New Approaches*, J. Nucl. Mater., **239**, 61 (1996).

60. H. Kanasaki, T. Okubo, I. Satoh, M. Koyama, T. R. Mager, and R. G. Lott, *Fatigue and Stress Corrosion Cracking Behaviors of Irradiated Stainless Steels in PWR Primary Water*, in Proc. 5th Int. Conf. on Nuclear Engineering, May 26-30, Nice, France (1997).

61. T. Tsukada, Y. Miwa, H. Nakajima, and T. Kondo, *Effects of Minor Elements on IASCC of Type 316 Model Stainless Steels*, in Proc. 8th Int. Symp. on Environmental Degradation of Materials in Nuclear Power Systems - Water Reactors, S. M. Bruemmer, ed., American Nuclear Society, La Grange Park, IL, pp. 795-802 (1997).

62. T. Yonezawa, K. Fujimoto, H. Kanasaki, T. Iwamura, S. Nakada, K. Ajiki, and K. Sakai, *SCC Susceptibility of Irradiated Austenitic Stainless Steels for PWR*, in Proc. 8th Int. Symp. on Environmental Degradation of Materials in Nuclear Power Systems - Water Reactors, S. M. Bruemmer, ed., American Nuclear Society, La Grange Park, IL, pp. 823-830 (1997).

63. M. Kodama, S. Nishimura, Y. Tanaka, S. Suzuki, K. Fukuya, S. Shima, K. Nakata, and T. Kato, *Mechanical Properties of Various Kinds of Irradiated Austenitic Stainless Steels*, in Proc. 8th Int. Symp. on Environmental Degradation of Materials in Nuclear Power Systems - Water Reactors, S. M. Bruemmer, ed., American Nuclear Society, La Grange Park, IL, pp. 831-838 (1997).

64. H. M. Chung, J.-H. Park, W. E. Ruther, J. E. Sanecki, R. V. Strain, and N. J. Zaluzec, *Fabrication-Related Impurity Contamination and Stress Corrosion Cracking of Austenitic Stainless Steel Core-Internal Components*, in Proc. 8th Intl. Symp. on Environmental Degradation of Materials in Nuclear Power Systems - Water Reactors, S. M. Bruemmer, ed., American Nuclear Society, La Grange Park, pp. 846-856 (1997).

65. J. M. Cookson, G. S. Was, and P. L. Anderson, *Oxide-Induced Initiation of Stress Corrosion Cracking in Irradiated Stainless Steel*, Corrosion **54**, 299 (1998).

66. H. M. Chung, W. E. Ruther, and R. V. Strain, *Slow Strain Rate Tensile Testing of Model Austenitic Stainless Steels Irradiated in the Halden Reactor*, in Environmentally Assisted Cracking in Light Water Reactors, Semiannual Report, July-December 1998, NUREG/CR-4667, Vol. 27, ANL-99/11, pp. 28-38 (October 1999).

67. S. M. Bruemmer et al., *Critical Issue Reviews for the Understanding and Evaluation of Irradiation–Assisted Stress Corrosion Cracking*, EPRI TR-107159, Electric Power Research Institute, Palo Alto, CA (1996).

68. M. L. Herrera, et al., *Evaluation of the Effects of Irradiation on the Fracture Toughness of BWR Internal Components*, in Proc. ASME/JSME 4th Intl. Conf. on Nucl. Eng. (ICONE-4) Vol. 5, A. S. Rao, R. M. Duffey, and D. Elias, eds., American Society of Mechanical Engineers, New York, pp. 245-251 (1996).

69. W. J. Mills, *Fracture Toughness of Type 304 and 316 Stainless Steels and their Welds*, Intl. Mater. Rev. **42**, 45-82 (1997).

70. P. J. Maziasz and C. J. McHargue, *Microstructural Evolution in Annealed Austenitic Steels during Neutron Irradiation*, Int. Met. Rev. **32**, 190 (1987).

71. P. J. Maziasz, *Overview of Microstructural Evolution in Neutron-Irradiated Austenitic Stainless Steels*, J. Nucl. Mater. **205**, 118-145 (1993).

72. F. A. Garner, *Evolution of Microstructures in Face-Centered Cubic Metals during Neutron Irradiation*, J. Nucl. Mater. **205**, 98-111 (1993).

73. J. Dufresne, B. Henry, and H. Larsson, *Fracture Toughness of Irradiated AISI 304 and 316L Stainless Steels*, in Effects of Radiation on Structural Materials, ASTM STP 683, J. A. Sprague and D. Kramer, eds., American Society for Testing and Materials, Philadelphia, pp. 511-528 (1979).

74. C. Picker, A. L. Stott, and H. Cocks, H., *Effects of Low-Dose Fast Neutron Irradiation on the Fracture Toughness of Type 316 Stainless Steel and Weld Metal*, in Proc. Specialists Meeting on Mechanical Properties of Fast Reactor Structural Materials, Chester, UK, Paper IWGFR 49/440-4 (1983).

75. F. H. Huang, *The Fracture Characterization of Highly Irradiated Type 316 Stainless Steel*, Int. J. Fracture **25**, 181-193 (1984).

76. J. Bernard and G. Verzeletti, *Elasto-Plastic Fracture Mechanics Characterization of Type 316H Irradiated Stainless Steel up to 1 dpa*, in Effects of Radiation on Materials: Twelfth Intl. Symp., ASTM STP 870, F. A. Garner and J. S. Perrin, eds., American Society for Testing and Materials, Philadelphia, pp. 619-641 (1985).

77. W. J. Mills, *Irradiation Effects on the Fracture Toughness of Austenitic Fe-Cr-Ni Alloys*, HEDL-TME-82-17, Hanford Engineering Development Laboratory (1985).

78. W. J. Mills, *Fracture Toughness of Irradiated Stainless Steel Alloys*, Nucl. Technol. **82**, 290-303 (1988).

79. D. J. Michel and R. A. Gray, 1987, *Effects of Irradiation on the Fracture Toughness of FBR Structural Materials*, J. Nucl. Mater. **148**, 194-203 (1987).

80. P. Ould, P. Balladon, and Y. Meyzaud, *Bull. Cercle Etud. Metaux* **15**, 31.1-31.12 (1988).

81. E. V. Van Osch, M. G. Horsten, and M. I. De Vries, *Fracture Toughness of PWR Internals,* ECN Contribution to CEC Contract on PWR Internals–Part 2 (ETNU/CT/94/0136–F), ECN-I-97-010 (71747/NUC/EvO/mh/006274), Netherlands Energy Research Foundation ECN, Petten, the Netherlands (1997).

82. T. H. Hughes and E. E. Gruber, *Development of Hot–Cell J–R Test Facility,* in Environmentally Assisted Cracking in Light Water Reactors Semiannual Report July 1996–December 1996, NUREG/CR-4667, Vol. 23, ANL-97/10, pp. 42–52 (1997).

83. E. E. Gruber and O. K. Chopra, *Fracture Toughness J–R Test of Austenitic Stainless Steels Irradiated in Halden Reactor,* in Environmentally Assisted Cracking in Light Water Reactors Semiannual Report January 1997–June 1997, NUREG/CR-4667, Vol. 24, ANL-98/6, pp. 54–65 (1998).

84. E. E. Gruber and O. K. Chopra, *Fracture Toughness J–R Test of Austenitic Stainless Steels Irradiated in Halden Reactor,* in Environmentally Assisted Cracking in Light Water Reactors Semiannual Report July 1998–December 1998, NUREG/CR-4667, Vol. 27, ANL-99/11, pp. 39–45 (Oct. 1999).

85. A. L. Hiser, *Fracture Toughness Chracterization of Nuclear Piping Steels,* NUREG/CR-5118, MEA-2325, Materials Engineering Associates, Inc., Lanham, MD (1989).

86. G. M. Wilkowski, et al, *Degraded Piping Program – Phase II, Semiannual Report,* NUREG/CR-4082, Vol. 2 (1985).

87. M. G. Vassilaros, R. A. Hays, and J. P. Gudas, *Investigation of the Ductile Fracture Properties of Type 304 Stainless Steel Plate, Welds, and 4–Inch Pipe,* in Proc. 12th Water Reactor Safety Information Meeting, NUREG/CP-0058, Vol. 4, U.S. Nuclear Regulatory Commission, pp. 176–189 (1985).

88. W. E. Ruther, W. K. Soppet, and T. F. Kassner, *Corrosion Fatigue of Alloys 600 and 690 in Simulated LWR Water,* NUREG/CR-6383, ANL-95/37 (April 1996).

89. W. E. Ruther, W. K. Soppet, and T. F. Kassner, *Environmentally Assisted Cracking of Alloys 600 and 690 in Simulated LWR Water,* in Environmentally Assisted Cracking in Light Water Reactors, Semiannual Report, July 1997–December 1997, NUREG/CR-4667 Vol. 25, ANL-98/18, pp. 42–75 (Sept. 1998).

90. W. E. Ruther, W. K. Soppet, T. F. Kassner, and W. J. Shack, *Environmentally Assisted Cracking of Alloys 600 and 690 in Simulated LWR Water,* in Environmentally Assisted Cracking in Light Water Reactors, Semiannual Report, January 1998–June 1998, NUREG/CR-4667 Vol. 26, ANL-98/18, pp. 25–32 (March 1999).

91. W. E. Ruther, W. K. Soppet, T. F. Kassner, and W. J. Shack, *Environmentally Assisted Cracking of Alloys 600 and 690 in Simulated LWR Water,* in Environmentally Assisted Cracking in Light Water Reactors, Semiannual Report, July 1998–December 1998, NUREG/CR-4667 Vol. 27, ANL-99/11, pp. 45–54 (Oct. 1999).

92. F. P. Ford, *Quantitative Prediction of Environmentally Assisted Cracking*, Corrosion, **52**, 375–395 (1997).

93. F. P. Ford, D. F. Taylor, P. L. Andresen, and R. Ballinger, *Corrosion–Assisted Cracking of Stainless and Low–alloy Steels*, EPRI NP–5064s, Electric Power Research Institute, Palo Alto, CA (Feb. 1987).

94. T. Shoji, *Quantitative Prediction of Environmentally Assisted Cracking Based on Crack Tip Strain Rate*, in Proc. Conf. on Predictive Capabilities in Environmentally–Assisted Cracking, R. Rungta, ed., PVP Vol. 99, American Society of Mechanical Engineers, New York, pp. 127–142 (1985).

95. W. J. Shack and T. F. Kassner, *Review of Environmental Effects on Fatigue Crack Growth of Austenitic Stainless Steels*, NUREG/CR–6176, ANL–94/1 (May 1994).

96. J. D. Gilman, R. Rungta, P. Hinds, and H. Mindlin, *Corrosion–Fatigue Crack–Growth Rates in Austenitic Stainless Steels in Light Water Reactor Environments*, Int. J. Pressures Vessels and Piping, **31**, 55–68 (1988).

97. E. D. Eason, E. E. Nelson, and J. D. Gilman, *Technical Basis for a Revised Fatigue Crack Growth Rate Reference Curve for Ferritic Steels in Light Water Reactor Environments*, in Welding Research Council Bulletin 404, Report No. 3, pp. 38–51 (1995).

98. W. E. Ruther, W. K. Soppet, and T. F. Kassner, *Effect of Temperature and Ionic Impurities at Very Low Concentrations on Stress Corrosion Cracking of AISI 304 Stainless Steel*, Corrosion **44**, 791-799 (1988).

99. W. E. Ruther, W. K. Soppet, and T. F. Kassner, *Influence of Environment and Temperature on Crack Growth of Type 304 SS under Cyclic Loading in Simulated BWR-Quality Water*, in Environmentally Assisted Cracking in Light Water Reactors, Annual Report, October 1983–September 1984, NUREG/CR–4287 ANL–85–33, pp. 110–114 (1985).

2. TITLE AND SUBTITLE

Environmentally Assisted Cracking in Light Water Reactors.

Semiannual Report January 1999—June 1999

3. DATE REPORT PUBLISHED

MONTH	YEAR
July	2000

4. FIN OR GRANT NUMBER

W6610

5. AUTHOR(S)

O. K. Chopra, H. M. Chung, E. E. Gruber,

T. F. Kassner, W. E. Ruther, W. J. Shack,

J. L. Smith, W. K. Soppet, and R. V. Strain

6. TYPE OF REPORT

Technical; Semiannual

7. PERIOD COVERED *(Inclusive Dates)*

January 1999—June 1999

8. PERFORMING ORGANIZATION – NAME AND ADDRESS *(If NRC, provide Division, Office or Region, U.S. Nuclear Regulatory Commission, and mailing address; if contractor, provide name and mailing address.)*

Argonne National Laboratory
9700 South Cass Avenue
Argonne, IL 60439

9. SPONSORING ORGANIZATION – NAME AND ADDRESS *(If NRC, type "Same as above"; if contractor, provide NRC Division, Office or Region, U.S. Nuclear Regulatory Commission, and mailing address.)*

Division of Engineering Technology
Office of Nuclear Regulatory Research
U.S. Nuclear Regulatory Commission
Washington, DC 20555-0001

10. SUPPLEMENTARY NOTES

M. B. McNeil, NRC Project Manager

11. ABSTRACT (200 words or less)

This report summarizes work performed by Argonne National Laboratory on fatigue and environmentally assisted cracking (EAC) in light water reactors (LWRs) from January 1999 to June 1999. Topics that have been investigated include (a) environmental effects on fatigue S–N behavior of primary pressure boundary materials, (b) irradiation–assisted stress corrosion cracking (IASCC) of austenitic stainless steels (SSs), and (c) EAC of Alloys 600 and 690. Fatigue tests have been conducted to study the effects of water chemistry on the fatigue life of austenitic SSs in LWR environments. Existing fatigue S–N data have been evaluated to establish the effects of temperature, dissolved oxygen, and strain rate on the fatigue life of these steels. Slow-strain-rate tensile tests and posttest fractographic analyses were conducted on several model SS alloys irradiated to $\approx 0.9 \times 10^{21}$ n·cm^{-2} (E > 1 MeV) in He at 289°C in the Halden reactor. The results have been used to determine the influence of alloying and impurity elements on the susceptibility of these steels to IASCC. Fracture toughness J–R curve tests were also conducted on two heats of Type 304 SS that were irradiated to ≈ 0.3 and 0.9×10^{21} n·cm^{-2} in the Halden reactor. Crack-growth-rate tests have been conducted on compact-tension specimens of Alloy 690 under cyclic loading to evaluate the enhancement of crack growth rates of these alloys in LWR environments.

12. KEY WORDS/DESCRIPTORS *(List words or phrases that will assist researchers in locating this report.)*

Corrosion Fatigue

Crack Growth

Irradiation–Assisted Stress Corrosion Cracking

Radiation–Induced Segregation

Stress Corrosion Cracking

Types 304, 304L, 316, and 316NG Stainless Steel

Alloys 600 and 690

13. AVAILABILITY STATEMENT

Unlimited

14. SECURITY CLASSIFICATION

(This Page)

Unclassified

(This Report)

Unclassified

15. NUMBER OF PAGES

16. PRICE

UNITED STATES
NUCLEAR REGULATORY COMMISSION
WASHINGTON, D.C. 20555-0001